Title- Modulation of implanted aortic scaffold- involvement of ECM and immune proteins

Author's list

1. Debashish Banerjee[#] (debashish.banerjee@transplant.gu.se)

2. Nikhil B. Nayakawde (nikhil.nayakawde2010@gmail.com)

3. Deepti Antony[*] (deepti.antony@transplant.gu.se)

3. Meghshree Deshmukh[*] (meghshreed@gmail.com)

4. Sudip Ghosh[‡a] (sudip.ghosh@med.lu.se)

4. Carina Sihlbom[‡b] (carina.sihlbom@gu.se)

5. Uzair Ul Haq (qazi_raheel2003@yahoo.com)

6. Michael Olausson (michael.olausson@transplant.gu.se)

[#] Corresponding author

[*] and [‡] Contributed equally to this work

1, 2, 3 and 5- Laboratory for Transplantation and Regenerative Medicine, Sahlgrenska University Hospital, Gothenburg University, Sweden; 4a- Proteomic Hematology, Lund Stem Cell Center, Lund University; 4b- Proteomics core facility, Sahlgrenska Academy, University of Gothenburg, Sweden and 6 -Department of Transplantation Surgery at Sahlgrenska Academy, University of Gothenburg and Sahlgrenska University Hospital, Gothenburg, Sweden.

Keywords

vascular scaffold, decellularization, syn/allogeneic, implant, extracellular matrix, immune cells

Abstract

The development of a suitable biological scaffold or implant is a pre-requisite for the functional development of organs including blood vessels. Biological scaffold prepared by physical or chemical agents cause damage to the extracellular matrix architecture and induce immune response after scaffold implantation/engraftment. During the current study, taking advantage of different host tissue environments (subcutaneous *vs* omentum), acellular scaffolds/implants

were prepared based on syngeneic *vs* allogeneic model of scaffold implantation (*in vivo* decellularization) and compared with chemically decellularized scaffolds. Employing molecular, proteomics, and histologic techniques, we confirmed that site-specific advantages exist in modulating the ECM as well as regulating the immune responses (macrophage and T-cells) to produce an acellular scaffold without the need for immunosuppressants. The current approach opens up the possibility to create tailor-made scaffolds for further use in the clinics with a potential for long term acceptability without eliciting adverse reactions in the host. The scaffolds prepared thus would open up a further possibility to build functional organs following cell engraftment.

Impact statement

During the current study an alternative strategy of preparing a scaffold by natural means was investigated which would also give an option to avoid the detrimental effect of chemicals used while preparing a biological scaffold. Understanding the cellular milieu of an implanted scaffold would help to modify the immunological trigger upon scaffold implantation, an aspect also studied during the current research. The infiltrating cells and their putative relationship with the biological scaffold could help the researcher to target immune cells to avoid scaffold/implant rejection. In a nutshell, the study carried out without any immunosuppressive agents could help further exploration of (a) alternative strategies for preparing biological scaffolds and (b) implantable sites as potential bioreactors with the aim to avoid any adverse immune reactions for further acceptance of the scaffold/implant post implantation.

Introduction

Transplantation of organs, cells, and tissues has proved to be lifesaving by restoring essential functions e.g. normal blood flow to vital organs (e.g. coronary heart and peripheral artery disease) by revascularization techniques like angioplasty, placement of a stent, or surgical bypass scaffolding. Both synthetic and blood vessels e.g. saphenous vein, internal thoracic artery, and radial arteries are often used as a conduit for revascularization as a regenerative measure or tissue engineering approach.

The main goal for tissue engineering of blood vessels is to create vascular scaffold identical to native vessels with the potentiality to support cell engraftment. The initial development of blood vascular scaffold **[1]** and refinement in terms of rapid endothelization and extracellular matrix (ECM) deposition **[2]** has helped tissue engineering technique to develop successful

blood vessels with minimum thrombosis, inflammation, and promotion of scaffold acceptance **[3, 4]**.

The usual chemical procedure used for the development of acellular biological scaffold (decellularization technology) **[5, 6]** has been reported to damage the extracellular matrix and elicit immunological reaction, immunologic incompatibility with limited mechanical tolerance **[7, 8]**. However, natural vascular scaffolds in comparison to synthetic scaffolds have certain advantages such as natural binding sites for cell adhesion (conserved native 3-D structure), improved biomimetic and biocompatibility stimulating colonization, promoting the proliferation of recruited cells. Furthermore, remodeling of the autologous vascular scaffolds *in vivo* which acquired native tissue architecture due to the maintenance of smooth muscle cells, extracellular matrix organization, and endothelial cells have been reported **[4, 9]**.

Selection of scaffold implantation sites like subcutaneous and omentum with unique cellular niche and different blood supply has been reported to support free structures for reconstructive purposes **[10-12]**. The uniqueness of the two sites for implantation has earlier been documented with the omentum rich in blood supply **[13]** whereas the subcutaneous site associated with low oxygen tensions **[14].**

Implantation of a biomaterial and its degraded by-product induces an immune reaction in the host which determines the outcome of the final integration and the biological performance of the implant. The host immune reactions following biomaterial implantation include amongst others blood-material interactions, provisional matrix formation, granulation tissue development, foreign body reaction, and fibrosis/fibrous capsule development deciding the development of acute or chronic reactions **[15].** The nature of the host immune cells e.g. macrophages depends on the immediate tissue niche of the biomaterials influencing the outcome of the tissue-specific innate and adaptive immune responses against biomaterials **[16].**

A modern scientific tool to assess biological scaffold includes mass spectrometric based quantitative proteomic analysis and bioinformatics prediction to identify and analyze proteins of the extracellular matrix **[17]** as well as an immune response after transplantation **[18].**

Based on proteomics and immunohistological tools, the dynamics of protein expression in the immediate niche of the implanted scaffolds were monitored during the current study. The findings from the current study could help us to better understand the remodeling of the implant as a result of the putative interaction between the ECM and the immune infiltrating cells, chose an alternative source of implantation, as well as manipulate the immunological target to minimize adverse immune reaction.

Materials and Methods

All reagents used were of analytical grade. Antibodies used are summarized in **Supplementary file (Tables 2A-2B).**

(A) Preparation of biological scaffold

Harvesting of aorta

Lewis and Norwegian Brown male (2.5 months age, weight ≈180-220 g, Janvier Labs, Germany) were housed and bred with food and water *ad libitum* at the Gothenburg University Experimental Biomedicine Center as per approved Animal Ethical Guideline (Göteborgs Djurförsöksetiska Nämnd, Ethical Number, 151/14).

Surgical preparation

The male Lewis and Brown Norway rats (aged 9-11 weeks) were prepared for surgery following anaesthesia. The rat was laid on the surgical table in dorsal recumbence and the ventral portion was sterilized using 70% ethanol. Using a midline incision under deep anesthesia, the aorta was harvested following ligation of branches.

Storage of harvested blood vessel

The harvested aorta was rinsed in phosphate- buffer saline (PBS) containing antibiotic (0.5% penicillin, 0.5% streptomycin), and antimycotic (0.5% amphotericin B) finally washed with PBS and water before freezing them at -150^{0}C within 4 h of death. Aortas were thawed overnight at 4°C and used either as donor normal (untreated aorta) or used for chemical decellularization before implantation as described below.

Chemical decellularization procedure of donor aorta

The decellularization steps were performed as reported earlier **[19]** at room temperature (20-24 °C) with slight modification using a closed-circuit system to minimize contamination. Each decellularization cycle consisted of a 7-hour treatment with 0.2% SDC (SDC; Sigma-Aldrich, St. Louis, MO, USA) with an alternate cycle of 7-8-hour treatment with glycerol mix solution (10% glycerol, 0.9% sodium chloride and 2 mM sodium-ethylene diaminetriacetic acid) with a wash with distilled water in between to remove cell debris as shown schematically in **Figure 1**. After the SDC cycle, washing was performed overnight with sterile water using an open system to drain out the wash continuously. A total of 5 cycles was given to achieve decellularization as assessed from DNA load and H&E staining.

Sterilization of chemically decellularized scaffold

The normal and decellularized donor aortic scaffold was sterilized by antibiotics-antimycotic solution and a pH-adjusted (pH- 7-7.4) solution of peracetic acid (2%) and ethanol (20%) for 4 hours at room temperature followed by DNase treatment as described in **Supplementary file** to achieve the recommended level of DNA load after decellularization **[20]**.

Upon confirmation of decellularization, the chemically-treated aortas were designated as decellularized aorta in comparison to the native untreated aorta, referred to as the donor decellularized and donor normal scaffold/implant in all subsequent sections **(Supplementary file- Table 1).**

(B) Transplantation and post-implantation biochemical study

Transplantation and harvesting of the aorta

Lewis female rats (n=6; 2.5 months age, weight ≈180-200 g, Janvier Labs, Germany) were used for the implantation of ≈1.5 -2 cm of sterilized donor normal and DC implants prepared earlier. The normal (LN and BNN) and decellularized donor (LDC and BNDC) scaffolds were placed under subcutaneous (S/C) and omentum route using 7/0 Prolene suture for implantation. To minimize the number of animals, the same animal was used for implantation at subcutaneous and omentum site (details are outlined in **Supplementary file, Methodology**. The nomenclature of the donor as well as implanted scaffolds is outlined in **Supplementary file- Table 1**).

The recipient Lewis rats were sacrificed after two months of scaffold implantation and the implants were harvested *in situ* and blood samples collected by cardiac puncture before the sacrifice of the animal. All operative procedure was performed according to the approved Animal ethical guidelines (Göteborgs Djurförsöksetiska Nämnd, Ethical Number, 151/14).

Processing of samples

The implanted scaffold for proteomics analysis (≈3-4 mm) and DNA isolation (≈1-1.5 mm) were snap-frozen in liquid nitrogen and stored at -150^{0}C whereas samples for gene expression (≈3-4 mm) were stored with RNALater at -80^{0}C. The scaffold samples for histological analysis (≈5-6 mm) were immediately fixed in formalin. The serum samples were prepared from collected blood and stored at -20^{0}C for further analysis.

Histological assessment

Tissue processing and staining

The donor non-transplanted (normal and DC scaffold after sterilization) and implants (collected from different sites) were fixed in formalin for a period of 48 h before paraffin embedding and

sectioning at 4 μM thickness. The 4 μM thickness paraffin section were deparaffinized (heating at 62^0C and subsequent xylene treatment), subsequently rehydrated in a decreasing grade of ethanol, and finally washed with distilled water. The sections were finally processed for H&E staining and immunohistochemical localization of different protein targets (ECM and immune cells).

Architectural preservation score of the decellularized aorta

The H&E stained sections were evaluated for structural integrity (architectural preservation) and nuclear loss (nuclear basophilia) by a pathologist (A.K.) using a Comprehensive method of masking tissues **[21]** with individual labeling of slides followed by Ordinal Data Measurements **[5].** The semi-quantitative evaluation of the tissue architecture was performed using a scoring represented as (1) complete breakdown of tissue, (2) marked disruption, 3) moderate disruption, (4) minimal disruption, and (5) no damage to cellular architecture.

Nuclear basophilia score of the decellularized aorta

A semi-quantitative nuclear loss score was performed representing nuclear basophilia (1) complete loss (100%), (2) substantial loss (70%), 3-moderate loss (50%), (4): minimal loss (30%), and (5) no loss of nuclear basophilia (0%) **[5].**

Inflammatory and fibrosis score

To monitor the degree of inflammation and fibrosis, a simple scoring system was used based on the following scoring criterion- (i) absent/ none-0, (ii) mild/weak- 1, (iii) moderate- 2 and (iv) severe/strong- 3.

Immunohistochemical assessment

Formalin-fixed paraffin sections (4 μM) were deparaffinized and subjected to heat mediated antigen retrieval for 25 min in 10 mM citrate buffer, pH 6. Sections were blocked with Candor Blocking solution+15% Normal Goat Serum for 45 min, probed with the primary antibodies diluted in low cross buffer (**Supplementary file- Table 2)**, washed 4 times with PBS-Tween 20 (0.05%), and probed for 1h with secondary antibody, conjugated with a fluorescent probe (see **Supplementary file, Table 1**). Finally, the air-dried slides were mounted in fluorescent mounting media containing DAPI (Fluoroshield, Cat. No. ab104139; Abcam) and imaged with a Leica Epifluorescence Microscope (DM5100). The overlapped images have been shown for clarity and localization of cells in the Results section.

Image acquisition and analysis

The image analyses were performed using the pipelines developed by the Imaging Core Facility, Gothenburg University **(Supplementary file- Image Analysis).** The image analysis involved the identification of (i) the area covered by target cells (immune cells) as well as the (ii) area stained (ECM).

During experimental acquisition, fluorescent images with 3 distinct configurations were taken named: Ch00 - nuclear staining, Ch01, and Ch02 depending on the immune markers or the ECM proteins and specified in the corresponding figure legends.

Proteomic Analysis

Sample Preparation

For proteome analysis, 3-4 mm of donor scaffolds and implants (n=6) were used. In total, twelve groups were selected for proteomic analysis **(Supplementary file- Table 1)**. The samples were homogenized in the lysis buffer (50 mM triethylammonium bicarbonate (TEAB), 2% sodium dodecyl sulfate (SDS), centrifuged, and supernatants transferred into new vials. Protein concentration was determined using Pierce™ BCA Protein Assay (Thermo Scientific). As reference samples, the controls Donor Lewis Normal (DLN) and Donor Brown Norway Normal (DBNN) were chosen to be analyzed in both TMT sets. Aliquots containing 30 µg of each sample and the references were digested with trypsin using the filter-aided sample preparation (FASP) method **[22]**. Peptides were collected by centrifugation. Digested peptides were labeled using TMT 11-plex isobaric mass tagging reagents (Thermo Scientific) according to the manufacturer instructions. The combined samples of each of the two TMT sets were pre-fractionated with basic reversed-phase chromatography (bRP-LC) using a Dionex Ultimate 3000 UPLC system (Thermo Fischer Scientific). Peptide separations were performed using a reversed-phase XBridge BEH C18 column (3.5 µm, 3.0x150 mm, Waters Corporation) and a linear gradient from 3% to 40% solvent B over 17 min followed by an increase to 100% B over 5 min. Solvent A was 10 mM ammonium formate buffer at pH 10.00 and solvent B was 90% acetonitrile, 10% 10 mM ammonium formate at pH 10.00. The 40 fractions were concatenated into 20 fractions, dried and reconstituted in 3% acetonitrile, 0.2% formic acid.

Liquid Chromatography-Tandem Mass Spectrometry Analysis

The fractions were analyzed on a QExactive HF mass spectrometer interfaced with the Easy-nLC1200 liquid chromatography system (Thermo Fisher Scientific). Peptides were trapped on an Acclaim Pepmap 100 C18 trap column (100 µm x 2 cm, particle size 5 µm, Thermo Fischer Scientific) and separated on an in-house packed analytical column (75 µm x 300 mm, particle size 3 µm, Reprosil-Pur C18, Dr. Maisch) using a gradient from 7% to 35% B over 76 min followed by an increase to 100% B for 8 min at a flow of 300 nL/min. The instrument operated

in a data-dependent mode where the precursor ion mass spectra were acquired at a resolution of 60 000, the 10 most intense ions were isolated in a 0.7 Da isolation window and fragmented using collision energy HCD settings at either 28 or 50. MS2 spectra were recorded at a resolution of 60 000, charge states 2 to 4 were selected for fragmentation and dynamic exclusion was set to 15 s with 10 ppm tolerance.

Protein Identification and Quantification

The data files for each TMT set were merged for identification and relative quantification using Proteome Discoverer version 2.2 (Thermo Fisher Scientific). The database search was performed using the Swissprot Rat Database (Oct 2018) using Mascot 2.5.1 (Matrix Science) as a search engine with a precursor mass tolerance of 5 ppm and fragment mass tolerance of 200 mmu. Tryptic peptides were accepted with zero missed cleavage, variable modifications of methionine oxidation and fixed cysteine alkylation, TMT-label modifications of N-terminal and lysine were selected. Percolator was used for the validation of identified proteins and the quantified proteins were filtered at 1% FDR and grouped by sharing the same sequences to minimize redundancy. Reporter ion intensities were quantified in MS2 spectra using the S/N values as abundances and normalized on the total protein abundance within the Proteome Discoverer 2.2 workflow. Only peptides unique for a given protein were considered for quantification and ratios were calculated by normalizing the samples with the reference samples DLN or DBNN. Only proteins quantified in all samples and relative standard deviation less than 25 percent in either syngeneic (LNSC, LNO, LDCSC, and LDCO) or allogeneic (BNNSC, BNNO, BNDCSC, and BNDCO) dataset were considered for comparisons among different sample groups. Proteins with two-fold expression changes were selected as up- or down-regulated.

Bioinformatics Analysis

Differences between two groups were analyzed using an independent samples t-test; p-values below 0.05 were considered statistically significant.

PPI network construction and module analysis

Employing the Search Tool for the Retrieval of Interacting Genes (STRING v.10.5) **[23]**, we built the PPI network of the identified proteins. The minimum required interaction score was set to 0.400 (medium confidence), and disconnected nodes (proteins with no known interactions) were not included in the view. Moreover, the MCODE plugin of Cytoscape (v.3.7.2) **[24]** was used to identify network modules with degree cutoff = 2, node score cutoff = 0.2, k-core = 2, and max. depth = 100. The topological features of the modules were determined *via* NetworkAnalyzer **[25]** and Cytohubba **[26]** plugins of Cytoscape to identify the

hub proteins. The hub proteins were mapped to the ECM and Immune responsive network modules. Pathway enrichment analyses of the networks or modules were performed through DAVID (v.6.8) **[27]** using KEGG **[28].** Benjamini-Hochberg's adjusted p-values < 0.05 were considered for statistically significant enrichment results. Gene Ontology (GO) enrichment analyses were also performed for terms related to the extracellular matrix (ECM) and immune responses.

Gene expression analysis

RNA Quantification and ddPCR

Tissue samples (scaffolds/implants) stored at -80^{0}C in RNALater were thawed, weighed, lyophilized, and cut into about 2-5 mg pieces and subjected to homogenization (4,0 m/s for 40 s, 2 cycles; Fastprep-24 5G, MP Biomedicals, CA). RNA was isolated using RNeasy micro kit (Qiagen, Cat No. 74004), measured using NanoDrop One (Thermo Scientific), integrity assessed (Agilent RNA 6000 Pico Kit, Agilent 2100 Bioanalyzer instrument), and used finally for cDNA conversion (Cat No. 1708891; iScript cDNA synthesis kit; BioRad).

ddPCR reactions were performed using QX200 droplet digital PCR system (BioRad) and TaqMan based hydrolysis probes **[29]**. Beta actin (Actb) reference gene was used for normalization (Rn.PT.39a.22214838.g, IDT) of the expression levels for the following genes: CD68 (dRnoCPE5149097, BioRad), CD163 (dRnoCPE5175377, BioRad), MRC1 (dRnoCPE5170185, BioRad), Nos2 (dRnoCPE5201373, BioRad) and IL-10 (dRnoCPE5172671, BioRad).

Briefly, each of the 20 µL reactions contained 1×ddPCR supermix for probes (Cat. No. 1863024, BioRad), 1 µL of either FAM or HEX primer-probe mix, and 2 µL of cDNA sample (~2 ng). Each reaction was mixed with 70 µL Droplet generation oil for probes (Cat. No. 1863005, BioRad), partitioned into about ≈20,000 droplets in Cartridges for QX100 droplet generator (Cat. No. 186-4008, BioRad) and Droplet generator DG8 gasket (Cat. No. 1863009, BioRad) in QX200 Droplet Generator (BioRad), transferred to 96-well plates (BioRad) and sealed. The PCRs were performed in a C1000 Touch Thermal Cycler (BioRad) with the following cycling conditions: 1× (95°C for 10 min), 40× (94°C for 30s, 55°C for 1 min), 1× (98°C for 10 min), 1× (4°C until the plate is read) with a ramp rate of 2°C/s. The fluorescence intensity of the individual droplets produced was measured with the QX200 Droplet Reader (BioRad) after overnight incubation of the plate at 4°C. The data analysis was done with Quantasoft (BioRad) software from the negative and positive droplet population with a

threshold applied manually for each well for respective genes. The target gene expression value was represented as copies/ng of input RNA as per Coulter **[30]**.

XY chromosome quantification

Tissue samples were used for DNA isolation (DNeasy blood and tissue kit, Qiagen, Cat. No. 69504) protocol, quantified using NanoDrop One (Thermo Fisher), and analyzed for detection of X and Y chromosome using X and Y chromosome-specific probes **(Supplementary file).**

Proteome Profiler of cytokines present in serum

The relative serum cytokine expression was measured using the Proteome Profiler Rat Cytokine Array Kit, column A (R&D Systems Inc., Minneapolis, MN, ARY008 using the manufacturer's instruction **(Supplementary file)**.

Statistical analysis

The data were statistically analyzed using GraphPad Prism v.8.4 (GraphPad Software, La Jolla, CA) and R. The statistical analysis carried out in each experiment is defined in the corresponding figure legend. Details are provided in the **Supplementary file**.

Data availability

1. The raw/processed data required to reproduce few of the findings could not be shared at this time due to technical or time limitations. The experimental data required to reproduce the findings from this study will be made available to interested investigators upon request.
2. The Mass spectrometry proteomics data have been deposited to the ProteomeXchange Consortium *via* the PRIDE **[31]** with the dataset identifier PXD021179.
3. The code for all imaging pipelines for Cell and Area work will be made publicly available *via* github upon acceptance of the manuscript. During the review process we can also send the code to reviewers *via* e.g. a zip folder.

Results

A schematic diagram showing the preparation of an acellular vascular scaffold and subsequent implantation in recipient rats is shown **(Figure 1)**.

Decellularization strategy- preparation of chemically modified scaffolds

We initially prepared a decellularized scaffold from donor Lewis (DLN) and donor Brown Norway (DBNN) aorta and confirmed the preparation of a donor decellularized scaffold

(DLDC and DBNDC) by measurement of DNA content by Picogreen assay. The load of tissue DNA in the decellularized scaffold was below 10 ng and was significantly lesser than corresponding untreated samples ($^{\star\star\star}p<0.001$) **(Supplementary figure 1).**

Semi-quantitative histological scoring also confirmed the acellularity or nuclear basophilia (≈79.31%, $p^{\star\star}<0.01$, **Figures 2A and 2B, Supplementary figure 2**) as well as the tissue architecture (16.67%, $p^{\star}<0.05$, **Figures 2A and 2C, Supplementary figure 2**) of the donor decellularized scaffolds, DLDC and DBNDC to be significantly lesser than the donor normal scaffolds, DLN and DBNN.

In terms of the nuclear basophilia, the donor normal syngeneic, and allogeneic implants placed in the subcutaneous (LNSC- 62.07%, $^{\star}p<0.05$; and BNNSC- 58.62%, $^{\star}p<0.05$) and omentum (LNO- 72.42%, $^{\star\star}p<0.01$ and BNNO- 72.42%, $^{\star\star}p<0.01$) had significantly reduced nuclear basophilia compared to the donor normal scaffolds (DLN and DBNN). However, the basophilia scores for the decellularized implants were identical to the donor decellularized scaffolds. The architecture of the syngeneic and allogeneic implants placed in the subcutaneous route (LNSC and BNNSC) was not altered compared to the donor control, DLN, and DBNN. However, the omentum implants had significantly lower histological score compared to the normal donor, DLN and BNN (LNO ≈40%, $p^{\star\star}<0.01$ and BNNO ≈46.67%, $p^{\star\star\star}<0.01$) and subcutaneous, LNSC and BNNSC ($p^{\alpha}<0.05$) scaffolds.

However, the decellularized omentum implants showed significantly lower histological score (LDCO≈50%, $p^{\star\star}<0.01$, and BNDCO≈43.33%, $p^{\star\star}<0.01$) compared to the respective donor scaffolds (DLDC and DBNDC). The decellularized subcutaneous implants (LDCSC and BNDCSC) were at the same level as the respective donor scaffolds. The omental implants also showed a significant increase in the inflammation (LDCO and BNDCO-$^{\star}<0.05$) and fibrosis (BNNO- $p^{\star\star}<0.01$; LDCO and BNDCO- $p^{\star}<0.05$) score compared to the respective donor implants (**Supplementary figure 3**).

However, the endothelial lining was removed to a large extent even after careful washing while removing blood clots from normal untreated rat aorta and was also not visible in the decellularized scaffolds and the implants.

Furthermore, to characterize the origin of the infiltratory cells, we performed ddPCR analysis for Y-chromosome as a marker for any donor cells present. There were negligible donor cells in the form of the Y-chromosome present in all the transplanted groups suggesting efficient natural decellularization *in vivo* **(Supplementary figure 4).**

Proteomic analysis of syngeneic and allogeneic scaffolds following implantation

To study the differential expression of the protein after implantation, the normal and decellularized scaffolds/implants were subjected to 11-plex TMT-based LC-MS/MS-based proteomic analysis (**Supplementary figures 5A- B**). 1863 identified proteins (1% false discovery rate) were filtered for downstream analysis with a relative standard deviation of less than 25 (**Supplementary excel file**). The proteins were further analysed for the nature and reproducibility of the transplanted samples wherein we performed a principal component analysis (PCA) of the normalized protein intensity data. The implanted groups showed clear differentiation in PCA space with regards to both the route (subcutaneous, SC; omentum, O) and the nature of transplantation (syn- or allogeneic) due to homology and unique specificity (**Supplementary figure 5C**). The identified proteins also showed excellent reproducibility between replicate runs between the route and nature of transplantations (**Supplementary figure 5D**). The normal and decellularized samples of both syngeneic (Lewis-Lewis) and allogeneic (Brown Norway-Lewis) implants also significantly correlated among themselves (**Supplementary figure 5E**). The expression pattern was dynamic in the transplanted groups (**Supplementary figure 5F**). About ≈88 % of proteins were found to be common between syngeneic and allogeneic implantation suggesting maintenance of proteome stability in the transplanted scaffolds (**Supplementary figure 5G**).

Analysis of extracellular matrix protein organization after syngeneic and allogeneic implantation

ECM enriched proteins were further examined for their effect following syngeneic and allogeneic scaffold implantation at different sites. The expression of ECM proteins was quite distinct in normal and decellularized implants (**Supplementary figure 6A**). Both normal and decellularized implants shared route-specific homology. ECM proteins were significantly ($p<0.05$) enriched for GO categories related to proteinaceous extracellular matrix, extracellular matrix organization, disassembly, and extracellular fibril organization (**Supplementary figure 6B**). Furthermore, to determine the functional significance of ECM proteins in syngeneic and allogeneic set-up and to gain new insight into route-specific molecular features, we constructed a functional interaction network with the ECM proteins and visualized in cytoscape. Four functional modules or clusters were constructed using the MCODE plugin within cytoscape (**Figures 3A-D**). It is evident from the cluster organization that ECM components interact with each other to maintain the ECM stability and integrity in the case of both syn- and allogeneic

transplantation. In clusters 1, 2, and 4, ECM proteins interact with extracellular space proteins. Whereas in cluster 3, ECM and extracellular space proteins interact with extracellular fibril organization proteins. Some of these cluster members have a very dense connection and appears to regulate the cluster function. Ranked by degree and other 12 parameters in Cytohubba **[26]** and Network Analyzer app within Cytoscape, we identified the top eight proteins (Apoe, Apob, App, Fn1, Kng1, Sparc, Agt, and Actb) as hub proteins along with 4 relevant ECM proteins (Lamb2, Acta2, Ecm1, and Fndc1). Cluster 1 is enriched with five of the eight hub proteins (**Figure 3A**) whereas cluster 2 and 3 have one each (**Figures 3B and 3C**). These genes were Apoe, Apob, App, Fn1, Kng1, Sparc, and Agt. The heatmap represents the additional hub protein, Actb (**Figure 3E**). 5 proteins including 3 hub proteins were significantly increased in the normal syngeneic SC scaffolds, LNSC (App, Sparc, Lamb2 and Fndc1); and allogeneic SC scaffolds, BNNSC (Fndc1). In the omentum, the normal allogeneic scaffold (BNNO) showed enhanced expression for 4 proteins (Fn1, Actb, Lamb2, and Ecm1) whereas the normal syngeneic scaffold (LNO) showed 2 proteins each having either up (Sparc, Agt) or downregulated expression (Fn1, Ecm1). However, the decellularized scaffolds syngeneic (LDCO, LDSC) and allogeneic (BNDCSC and BNDCO) scaffolds showed a reduction in the expression of the ECM proteins (**Supplementary proteomics file, Supplementary figures 6-7)**

Dynamics of immune protein expression in syngeneic and allogeneic scaffolds

The proteomic data was further interrogated to evaluate the effect of immune responses in the syngeneic and allogeneic scaffolds implanted at different sites. Functional interactions for the immune-related proteins were retrieved from the STRING database. The protein expression pattern for both immune response proteins and ECM was unique for the route (subcutaneous *vs* omentum) and nature of the scaffolds (normal untreated *vs* decellularized) implanted. Both the syngeneic and allogeneic implants at the subcutaneous site (LNSC, BNSC, LDSC, and BNDCSC) were able to keep the expression of immune-related proteins at a lower level in comparison to the omentum implants (LNO, BNO, LDO, and BNDCO). The allogeneic subcutaneous implants (BNNSC and BNDCSC) had significantly less expression level as that of the syngeneic implants (LNSC and LDCSC) for all of the immune-related proteins except Lyn, IL6st, and CD31 (**Figure 4)**. On the other hand, the omental implants (both normal and decellularized syngeneic and allogeneic) showed more up (C1s, C4, RT1-Aw2, CD31, Serping 1, Syk and C1qa) than down (Syk, CD4, Lyn, C1qa and C1s) regulation of immune-related proteins **Figure 4)**. The majority of the immune responsive proteins showed dynamic

expression and were mainly involved in the regulation of innate immune responses **(Supplementary figures 6C- 6D**). MCODE analysis resulted the top two clusters for immune-related proteins **(Figures 4A-B)**. Cluster 1 is enriched with six of the nine hub proteins **(Figure 4A)** whereas cluster 2 has three. In cluster 1, proteins with adaptive immune response interact with proteins having the function in the regulation of immune response, which, again interact with innate immune responsive proteins in cluster 2. The 9 significantly upregulated hub proteins, as revealed by Cytohubba and Network Analyser, were Serping1, C1qb, C1s, Syk, C1qc, CD4, Lyn, C1qa, and C4. The other immune markers identified were Mpeg 1, Rt1-Aw2, Il1rap, Il6st, Cd31, and Tgfb1. Out of the 9 significantly expressed HUB proteins, 6 proteins (Serping1, C1qb, C1s, C1qc, C1qa, and C4) were related to the complement system whereas rest 3 proteins (Syk, CD4, and Lyn) are involved in B and T-cell regulation (**Supplementary excel file**). In general, the immune proteins were not at a significantly higher level for most of the proteins detected and decellularized implants (both syngeneic and allogeneic) had more downregulated (8 proteins) than upregulated (5 proteins) in comparison to the normal untreated implants (6 proteins downregulated and 5 proteins being upregulated) at different sites (**Supplementary figures 6 and 8**).

Immunohistochemical localization of ECM markers following implantation

We found the presence of hub proteins from proteomic analysis including Fibronectin (Fn1), Actin (Actb), and Laminin (Lamb2) having the potential to regulate the cluster function due to their very dense connection as seen also from bioinformatics prediction. Fibronectin **(Figures 5A and 5B**), laminin, and actin (**Figures 5C-5E**) which also forms an integral component of the ECM were also monitored at the protein level by immunohistochemistry.

The percentage positive area for a particular ECM protein was expressed in terms of the particular staining being present over and above the calculated threshold **(Supplementary file-Methodology)**. In the case of the Fibronectin expression, the decellularized donor scaffolds (LDC- 6.957 folds, $^{\star\star}p<0.01$ and BNDC- 4.997 folds, $^{\star\star}p<0.01$) had a significantly higher expression compared to the normal scaffolds. There was also a significant increase in the Fibronectin expression in the normal implants placed in the omentum compared to the control group (LNO-5.454 folds, $^{\star}p<0.05$ and BNNO- 2.562 folds, $^{\star}p<0.05$). In contrast, there was no increase in Fibronectin expression for the decellularized implants (LDCSC, LDCO, BNDCSC, and BNDCO- **Figures 5A and 5B**). However, there was a significant increase in the allogeneic decellularized implants placed at the subcutaneous (BNDCSC- $^{\alpha}p<0.05$) and omentum

(BNDCO- $^{\beta}p<0.05$) route compared to the normal implants (BNNSC and BNNO). In the case of the two other ECM components, α-smooth muscle actin (**Figures 5C and 5D**) and laminin (**Figures 5C and 5E**), the level of normal and decellularized control scaffolds was identical in expression. The chemical decellularization process did not alter the ECM components unlike Fibronectin but was modulated to a varying degree depending on the genetic background of the implants and the route of the implantation.

In case of the α-SMA, all the implants showed reduced expression compared to the donor normal scaffolds (DLN and DBNN). The level of reduction was higher in both the syngeneic and allogeneic subcutaneous implants (LNSC-16.7 folds and BNNSC-12.737 folds; LDCSC-23.51 folds and BNDCSC- 14.849 folds $^{\star\star\star}p<0.001$) in contrast to the syngeneic and allogeneic omentum implants (LNO- 2.184 folds and BNNO-2.034 folds, $^{\star}p<0.05$; LDCO-4.01 folds, $^{\star\star}p<0.01$ and BNDCO- 2.333 folds, $^{\star}p<0.05$) which showed lesser reduction compared to the donor normal scaffolds. Moreover, the omental implants showed significantly higher expression compared to the normal counterpart at the same route (LNO and BNO; BNDCO- $^{\alpha}p<0.05$). The laminin expression also followed similar expression patterns as the α-smooth muscle actin for the donor scaffolds (DLN and DBNN *vs* DLDC and DLBNDC). The level of the syngeneic and allogeneic subcutaneous (LNSC- 5.355 folds and BNNSC-7.330 folds; LDCSC-29.935 folds) and omentum (BNDCO- 18.5 folds) implants were significantly reduced compared to the donor scaffolds ($^{\star}p<0.05$). However, the normal allogeneic omentum implant (BNNO, $^{\alpha\alpha}p<0.01$) expression level increased and the decellularized allogeneic subcutaneous implant (BNDCSC, $^{\alpha}p<0.05$) decreased compared to the normal subcutaneous implant (BNSC). The expression level of the allogeneic decellularized scaffold (BNDCO) was reduced ($^{\beta\beta}p<0.01$) compared to the normal allogeneic implants.

Immunohistochemical localization of inflammatory markers following implantation

Since macrophages have been indicated to play an important role in scaffold/implant acceptance, rejection or modulation, we further characterized the macrophage population at gene and protein level by digital PCR (**Figure 6)** and immunohistochemistry (**Figures 7-9**). The proteomics findings also indicated the involvement of the innate immune system **(Supplementary figure 6D)**.

The genomic expression pattern of the macrophage markers, CD68, CD163, MRC1 and iNOS showed significant expression in all the implants at a varying level (**Figures 6A-D**). The CD68

gene expression for the normal subcutaneous donor implants (LNSC and BNNSC) was identical to that of donor control scxaffolds irrespective of the genetic background whereas the omentum implants (LNO- 6.174 folds and BNNO-10.097 folds) showed significantly higher expression compared to the donor normal and subcutaneous implant ($p^{\star}<0.05$) (**Figure 6A**). The decellularized syngeneic (LDCSC- 28.980 folds and LDCO- 43.75 folds) and allogeneic implants (BNDCSC- 31.473 folds and BNDCO- 43.73 folds) had significantly higher expression ($p^{\star\star\star\star}<0.0001$) compared to their respective normal implants **(Figure 6A).** For the CD163 gene expression, the decellularized implants (LDCSC- 57.489 folds, LDCO- 85.914 folds, BNDCO- 24.093 folds) showed significantly higher expression compared to the normal implants ($p^{\star\star\star\star}<0.0001$). Also, the decellularized omental implants showed higher expression compared to the normal counterpart ($p^{\alpha\alpha}<0.01$). The expression for the normal omental implants (LNO- 43.921 folds and BNO- 9.017 folds, $p^{\star}<0.05$ was at a lesser but significantly higher than the respective normal control (DLN and BNN) **(Figure 6B)**.

The expression pattern of MRC-1 gene was identical to that of the CD163 gene with the normal (LNO- $p^{\star}<0.05$ and BNNO- $p^{\star\star}<0.01$) implants and decellularized (LDCSC- $p^{\star\star\star\star}<0.0001$, BNDCSC- $p^{\star\star}<0.0001$, LDCO and BNDCO- $p^{\star\star\star\star}<0.0001$) implants showing both higher expression than the normal donor implants **(Figure 6C).**

The expression of iNOS was significantly increased in the decellularized omental implants (LDCO- $p^{\star}<0.05$ and BNDCO- $p^{\star\star}<0.01$) compared to the normal donor implants **(Figure 6D).** In terms of the anti-inflammatory cytokine, IL 10 the expression to a large extent mirrored the expression of macrophages with the normal (LNO- $p^{\star\star}<0.01$ and BNNO- $p^{\star\star}<0.001$) and decellularized implants (LDCO- $p^{\star\star}<0.01$, LDCSC- $p^{\star\star}<0.01$ and BNDCO- $p^{\star\star\star\star}<0.0001$) placed in the omentum showed significantly higher expression compared to the normal donor scaffolds (**Figure 6E**).

We performed multiplexing to characterize two protein targets by immunohistochemistry at the same time in the same tissue. We targeted to detect CD68 (pan macrophage) and CD163 (M2 macrophage); MHCII (M1 macrophage) and CD163 (M2 macrophage) and iNOS (M1 macrophage) and Arginase I (M2 macrophage) in our scaffold samples by immunohistochemistry (**Figures 7-9)** using appropriate positive control staining **(Supplementary figure 9).**

The expression of the pan, M1, and M2 macrophage markers was determined by dual staining and the expression level monitored as described under the **Supplementary file** (**Methodology**-Image acquisition and analysis). The percentage of positive cells for a particular marker was

expressed in terms of the nucleated cells with particular staining. Both the subcutaneous and omentum scaffolds showed an identical level of expression of pan macrophage marker, CD68 with the decellularized scaffold (≈21-23 fold; $p^{★★}<0.01$) showing higher expression compared to the normal scaffold (≈13-18 fold; $p^{★}<0.05$) (**Figures 7A and 7B**).

The CD163 expression also paralleled the CD68 expression albeit at a lesser level (≈1.5- 2 folds lesser, $p^{★}<0.05$). However, there was no difference in CD163 expression in different scaffolds (normal *vs* decellularized) placed at different sites (subcutaneous *vs* omentum) (**Figures 7A and 7C**) as well as co-expression of both CD68 and CD163 markers (**Figures 7A and 7D**). The CD68 and CD163 co-expression level also mirrored the CD163 expression pattern under different routes of implantation and nature of the implants. However, the level of co-expression was lesser than CD163 expression (≈1.5- 2 folds lesser, $p<0.05$) indicative of the presence of other macrophage markers.

Subsequently, we also monitored for the expression of MHCII as a potential M2 marker in the different implants along with CD163 expression (**Figure 8**). We could detect the presence of MHC II macrophages only in the decellularized omentum implants and was significantly higher (LDCO- 8.511 folds and BNDCO- 5.295 folds, $p^{★}<0.05$) than the donor control scaffolds. The co-expression of CD163 and MHCII expression (**Figure 8A and 8B-8D**) was mainly found in the omental (BNNO- 5.56 folds, $p^{★}<0.05$; LDCO- 7.758, $p^{★★}<0.01$ and BNDCO- 8.464 folds, $p^{★}<0.05$) along with the subcutaneous (LDCSC- 7.797, $p^{★}<0.05$) implants.

Also, we performed immunolabelling for two additional macrophage markers, iNOS (M1 macrophage) and Arginase I (M2 macrophage). The expression of M2 macrophage, Arginase I (**Figures 9A-9B**) was found mainly in the allogeneic (BNNSC- 2.569 folds, $p^{★}<0.05$ and BNNO- 3.963 folds, $p^{★}<0.05$) and decellularized syngeneic (LDCO- 3.061 folds, $p^{★}<0.05$) implants. The expression of the M1 macrophage, iNOS was however weak **(Figures 9A-9C).** In the syngeneic (LNSC- 1.934 folds, $p^{★}<0.05$ and LDCSC- 1.875 folds, $p^{★}<0.05$) implants, iNOS expression was upregulated but was downregulated in the case of the syngeneic decellularized omentum implants ($p^{\alpha}<0.05$-LDCO) compared to the similar implants at the subcutaneous site. The co-expression of Arginase I and iNOS could not be established.

Furthermore, monitoring for T-cells- $CD3^{+}$, $CD4^{+}$, and $CD8^{+}$ cells revealed infiltration mainly around the implants with few cells present also in the lumen of the implants (**Figure 10**). Histological comparisons of allogeneic and syngeneic implants earlier revealed identical cell infiltrations **(Figure 2 and Supplementary figure 3)**. By immunohistological localization, we

could identify specific immune markers with $CD3^+$, $CD4^+$, and $CD8^+$ cells. The expression of a pan T-cell marker, CD3 was not evident in the normal syngeneic and allogeneic implants (LNSC, BNSC, and LNO) but in the normal allogeneic implant at the omentum route (BNNO) where it was significantly upregulated (3.678 folds, ★$p<0.05$) in comparison to the donor normal aorta (DBNN). All the decellularized implants from the subcutaneous and omentum route except the syngeneic omentum implant (LDCO) showed significant upregulation of the CD3 expression compared to the respective donor normal implants (LDCSC- 5.032 folds and BNDCSC -6.358 folds, ★★$p<0.01$, BNDCO-3.918 folds, ★$p<0.05$) (**Figures 10A and 10C i**). The expression of the T-cell markers, CD4 and CD8 were also found to have a varied expression with CD4+ cells having ≈30-50 fold increase in the expression compared to the CD8+ cells of the same group (**Figures 10B and 10C ii-iii**). There were no differences between the syngeneic and allogeneic implants at any route of implantation (subcutaneous *vs* omentum with regards to the CD4 expression and was significantly upregulated compared to the donor normal aorta (5.771 -7.941 folds, ★★$p<0.01$ and 8.483- 10.503 folds, ★★$p<0.001$) (**Figures 10B and 10C ii**).

CD8 expression on the other hand was expressed at a much lesser level and showed inconsistent expression within the normal implant groups. All the decellularized implants however showed enhanced expression compared to the donor normal implants (2-5.4 folds, ★$p<0.05$ and 2.182 folds, ★★$p<0.01$) (**Figures 10B and 10C iii**).

The relative level of cytokines and chemokines was monitored using Proteome Profiler Rat Cytokine Array Kit, Panel A. The serum from recipient female Lewis mice with normally implanted scaffolds (syngeneic – LN and allogeneic – BN) and decellularized implanted scaffolds (syngeneic – LDC and allogeneic – BNDC) was compared with that of a female Lewis mouse for cytokine and chemokine presence at the end of 2 months. Only 5 cytokines out of 29 cytokines could be detected over and above the negative spots present in the array membranes- sICAM, LIX, L-Selectin, RANTES CCL5, and CXCL7. However, the levels of the cytokines were unchanged and similar to that of the control of sham rats. The expression pattern of cytokines is indicative of the absence of antibody-mediated rejection following scaffold implantation.

Discussion

Despite the drawbacks, biological scaffold prepared by decellularization technology has been successfully used to recreate various types of tissues and organs including the circulatory

system, and subsequently repopulate with a patient's cells to produce a personalized vascular scaffold **[4, 32].**

The current work highlight the refinement in the preparation of the blood vascular scaffold using the body's natural immune response and tissue remodeling capacity in a rat model of aortic syngeneic and allogeneic implantation. As a source of the acellular scaffold, allogenic biomaterials have certain advantages such as maintenance of native tissue composition, architecture, remodeling ability, and regenerate a host tissue while circumventing the immune responses **[33]**. However, the allogeneic scaffold/implant is also encountered with adverse immune responses driven by the type and genetic mismatch of scaffolds **[34]**. The development of an acellular scaffold by natural means could help overcome the problem associated with synthetic, biological scaffolds as well as allogeneic scaffolds owing to minimizing of unfavorable immune responses by selecting appropriate routes. During the study, we tried to utilize the body's natural ability to act as a tissue bioreactor to prepare biological implants/scaffold following implantation.

We prepared scaffold initially by chemical decellularization using an alternate cycle of SDC and Glycerol/EDTA mix to achieve an acellular state in tune with reported literature **[20]**. The chemically decellularized scaffolds showed loss of tissue architecture indicative of the deleterious effect of chemical decellularization **[35, 36].** Subsequently, we also prepared an acellular scaffold by placing aortic scaffold separately at subcutaneous and omentum site. To monitor the fate of syngeneic (Lewis- Lewis) and allogeneic (BN- Lewis) implants following *in vivo* implantation, donor normal and decellularized/acellular scaffolds were placed as a free-floating implant with no blood vessel anastomosis subcutaneously and in omentum. The implanted scaffolds behaved uniquely according to the route of implantation with typical histological and immunological features which was monitored at the tissue level by genomics and protein characterization. The proteomics findings were followed by the predictive outcome of the interaction of different proteins by bioinformatics tool which indicated the involvement of unique and distinct ECM proteins present in clusters participating in the interaction with extracellular space and extracellular fibril organization proteins. The difference in nature of the scaffold and route of implantation was reflected from the hub ECM and immune proteins expression with the subcutaneous implants showing more uniform expression of ECM and immune-related proteins compared to the omentum implants. The ECM protein exhibited unique route-specific expression which was however not strictly dependent on the initial chemical nature of the scaffold i.e. either normal or decellularized. ECM proteins like Fibronectin 1 (Fn1) and laminin (Lamb2) were found to be

upregulated in donor syn- and allogeneic samples whereas the expression was attenuated in decellularized scaffolds. A marked increase in the expression of vascular laminins and fibronectin is a common phenomenon in early syn- and allogeneic transplantation and may trigger lymphocyte recruitment at the implantation site **[37]**. This may be the reason for the ensuing immune responses observed irrespective of the genetic background of the subcutaneous and omentum implants. Extracellular Matrix Protein 1 (Ecm1) also showed a similar expression pattern, up-regulated mainly in normal tissues irrespective of origin (syngeneic *vs* allogeneic). Fibronectin type III domain-containing protein (Fndca), which is associated with G protein signaling is upregulated in general. Alpha actin (Acta2) which is normally associated with chronic rejection in all scaffolds **[38]** was not up-regulated in all the transplanted samples studied. The deposition of a fibrous capsule around decellularized ECM based scaffolds which normally elicits immune response limiting tissue remodeling and regenerative potential **[6]**, was mainly limited to the omental implants. The chemical decellularization process used by us mostly preserved the ECM components as seen from the immunohistochemical data. Due to decellularization, ECM epitopes got exposed to the antibodies used during our experiment and was probably the reason for being present at a higher level compared to the normal implants. Any additional enhancement in the decellularized implants could be attributed to the post-implantation modification. The proteomics findings pointed to the expression of the immune response proteins particularly the innate arm of the immune response with overlapping roles with the adaptive immune system. The immune markers detected were normally associated with complements, macrophages, and other immune cells with upregulation of the hub immune proteins in almost all the implants. However, some of the hub proteins were expressed preferentially in omental compared to the subcutaneous implants e.g. Serping1, C1qb, C1s, C1qc, C1qa, and C4, suggesting possible enhanced immune response in an omental milieu compared to the subcutaneous site. Anti-HLA class I antibodies are primarily implicated in acute rejection, whereas anti-HLA class II antibodies during late rejection. There was no upregulation in the allogeneic groups in comparison to the syngeneic scaffolds in the expression of MHC I molecules (RT1-Aw2) and also MHC II as seen later by immunohistochemistry. The complement proteins detected by proteomics can recognize danger signals generated by foreign particle e.g. intruding pathogens or danger-associated molecular patterns (DAMPs) presented by transplanted scaffolds **[39, 40]**. Complement component, C1q e.g. plays an important role in adaptive, and innate, immunity by interacting with both immunoglobulin and non-immunoglobulin activators, surface molecules, and clearance of cell debris as part of

the host defense system. The proteins like Syk, CD4, and Lyn have been implicated in the regulation of the adaptive and innate immune system. CD4, which is a membrane glycoprotein and a member of the immunoglobulin supergene family acts as a co-receptor in MHC class II-restricted T-cell activation by direct and indirect allorecognition **[41]**.

The tissue macrophages are one of the effector cells against injury and scaffold implantation carried out by modulating their own phenotype and surrounding cells. Using genomic analysis, we were able to detect pan, M1, and M2 macrophage subsets. The following subsets were detected (CD68- pan macrophage, CD163- M2 macrophage, MRC-1-M2 macrophage, and iNOS- M1 macrophage). We monitored the gene expression using β-actin as the reference gene, which was found to have more or less uniform expression across all the groups. We adapted the concept of Theoretical and Calculated ng input RNA **(Supplementary figure 10)** to normalize the reference gene which helped us to overcome the variability due to intra and inter group variability. **[30].** The target copies were then expressed in terms of the Calculated ng input RNA. Macrophages, which are an integral part of innate immune system, based on stimulation are classified as M1 (stimulated with interferon gamma, IFN-γ /lipopolysaccharide, LPS) and M2 (stimulated with interleukin-4, IL-4/interleukin-13, IL-13) macrophages. M1 macrophages are characterized by the high expression of MHC II and inducible nitric oxide synthase (iNOS) apart from the pan macrophage marker, CD68 whereas M1 macrophages are characterized by M2-associated genes such as arginase-1 (Arg1), Mrc1, CD163, and transforming growth factor beta 1 (TGF-β1) **[42].**

Using histochemical means, we could identify infiltrating macrophages and their phenotypes (CD68 -pan), MHCII -M1, iNOS -M1, CD163 -M2 and Arginase -M2 as a putative immune response after implantation. We focused on the identification of mainly two broad phenotypes of macrophages - M1 (pro-inflammatory) and M2 (anti-inflammatory) which are reported to regulate a host of inflammatory cytokines following implantation. The macrophage infiltration was predominantly located at the muscular area with fewer cells towards the lumen. The normal and decellularized omentum implants showed higher macrophage infiltration compared to the donor normal and subcutaneous implants. Although not significant the pan macrophage marker, CD68 expression was more in the decellularized implants at all routes but at the same level with normal implant for M2 macrophage, CD163. The expression for the M1 macrophage, MHCII was more prominent with the decellularized scaffolds whereas for M1 macrophage, iNOS there no uniform expression. The level of

expression for the M2 macrophage, Arginase I was significant in the normal allogeneic scaffold at either route. The critical role of M2 macrophages in the remodeling of engineered vessels after implantation due to the promotion of blood vessels, cell survival, and tissue regeneration has earlier been demonstrated **[43, 44].** The expression of macrophages particularly the M2 subsets indicates the type of immune response at the implantation site, indicating a favorable remodeling of the implanted scaffold.

An elevation of inflammatory markers and immune cell circulation has been reported as one of the main causes of all scaffold rejection promoted us to characterize tissue distribution of T-lymphocytes after implantation. To monitor the dynamics of the T-cell mediated rejection of implanted tissue, the presence of CD4+, CD8+ lymphocytes were detected along with the pan T-cell marker, CD3+ cells. Earlier CD4 protein was detected as a hub protein by proteomics. Moreover, the CD4/CD8 ratio is usually increased after solid allogeneic/alloscaffold transplantation and is an important index for evaluating immune rejection **[45, 46]**. Our study showed that the CD4+ and CD8+ cells in the syngeneic and allogeneic scaffolds were at an identical expression level. The presence of identical immune markers having the identical expression level at the subcutaneous and omentum site after implantation of syngeneic and allogeneic scaffolds suggests the involvement of a sterile inflammation at the implantation site which is produced irrespective of the genetic background. A statistically significant increase in the CD3+ cell was observed in all the decellularized implants (except the allogenic omentum implant) whereas an increase of CD4+ cells with a minimum infiltration of CD8+ cells was observed in both the normal and decellularized implants, suggestive of an absence of a strong T-cell-mediated immune response. The cellular infiltration reveals the nature of the infiltrate which is mainly CD4+ suggesting a delay in the rejection process. Both the syngeneic and allogeneic scaffolds showed well-preserved smooth muscles of blood vascular architecture and minimum intralumen cellular infiltrate with predominant mononuclear cell infiltration confined to the periscaffold space. Statistically significant increased proportion of CD4+ T lymphocytes in the implanted scaffolds when compared with controls as observed in our case could lead to improved scaffold outcome after implantation as has been seen with allogeneic transplant acceptance **[47].** The immune responsive proteins were mostly upregulated in normal allogeneic omental implants suggestive of a more localized immune response in the omentum. In syngeneic transplants, the pattern was quite distinct, with untreated syngeneic transplants showing upregulated immune responsive proteins in comparison to the

decellularized syngeneic transplants which showed down-regulated immune response proteins. We have seen earlier from gene expression study the increased expression of the anti-inflammatory cytokine, such as IL-10 in those scaffolds where there was higher macrophage infiltration, suggestive that these implants were also protected from damage due to excessive inflammation due to the potential crosstalk with a subpopulation of T cells such as regulatory (Tregs) **[48, 49]**.

In terms of the systemic immune response, there were no serum markers suggestive of any systemic inflammatory response. All the detected immune markers were found to be at the same level as the sham operated rats supporting a more favorable outcome of scaffold remodeling. We observed immune responses which were of moderate grade and were not severe to destroy the scaffold after implantation. This observation probably could be attributed to the anatomical feature of the blood vascular scaffold aorta having a large diameter, a marked absence of endothelial lining, the rigidity of the vessel as well as the implantation route selected. The subcutaneous site allowed minimizing the ensuing immune responses whereas the omentum prompted a more vigorous immune response which leads to alteration in the tissue architecture of the scaffold. The chemical decellularization strategy used was aimed to minimize the tissue architecture damage in terms of the ECM or triggering of an adverse immune reaction, which was to some extent again circumvented by choosing the subcutaneous route for implantation. The host response at different sites was similar to non-resorbableble foreign material characterized by low-grade chronic inflammation, negligible scaffold degradation, and fibrosis which was supported by our histology and immunohistological findings. The differential responses of tissue scaffolds placed subcutaneously **[50]** and in the omentum **[51]** have been reported earlier and points to the presence of innate immune cells particularly macrophages in the vicinity of the scaffold which could have contributed to the acellular state of both the syngeneic and allogeneic scaffolds placed at these routes during our study.

Biological scaffolds based on ECM have been shown to normally promote a macrophage switch from M1 to M2 cell population deciding the outcome of post-implantation. However, chemical decellularization can expose the ECM preventing the beneficial M2 response which can lead to scar tissue formation **[52, 53].** Moreover, alteration of the tissue-specific ECM composition following organ transplantation has also been reported **[54]**.

So, we decided to compare an acellular scaffold prepared without the involvement of chemicals but rather harnessing the body's natural immune defense system, which was in our case

predominantly the innate arm of the immune system i.e macrophages and partly adapted immunity through the involvement of CD4+ T-helper cells. From our histological findings, we could conclude that there was the maintenance of the typical smooth muscle architecture as well as the absence of a fibrous capsule around the normal and decellularized scaffold. However, we did not further process the normal aorta or the chemically decellularized aorta for further anastomosis study rather used to evaluate the alteration of the scaffold/ECM and ensuing immune responses after implantaton.

Concluding statement

The study opens up the possibility to utilize nature's immune machinery to produce an acellular scaffold that has the potential to support cellular support and growth due to the maintenance of ECM components as well as triggering moderate immune reactions after implantation. The importance of the development of a natural biological scaffold also stems from the concern with the fast commercialization of tissue-engineered organs e.g. decellularized tissue for clinical application in humans by FDA and CE which could possibly jeopardize patient's safety on the grounds of quality control and safety of transplantable organs **[55].** There are few limitations to this study though. Our study was based on a terminal time point of 2 months which did not allow for dynamic observations. We only used our implant as a free-floating scaffold without direct blood vascular anastomosis, limiting the potential of our developed scaffold as a graft. However, the main motive of our study was to develop a biological scaffold and to study the response of body's natural immune machinery against different implants at two pre-decided implant sites and the remodeling events subsequent to implantation.

Author contributions

Debashish Banerjee: Conceptualization, Methodology, Investigation, Writing - original draft **Nikhil B. Nayakawde:** Conceptualization, Methodology, Investigation. **Deepti Antony, Meghshree Deshmukh, Sudip Ghosh and Carina Silbohm:** Methodology, Investigation **Uzair Ul Haq:** Methodology and **Michael Olausson:** Methodology, Supervision, Funding acquisition.

Acknowledgements

The authors would like to thank Rafael Camacho, Center for Cellular Imaging, University of Gothenburg for developing the image analysis pipelines and Dr. Anikó Kovács (A.K.),

pathologist, Sahlgrenska University Hospital, University of Gothenburg for the Histological interpretation. The authors thank Dr. Goditha U. Premaratne for technical suggestions.

Funding Information

The research was financed by the Swedish Government LUA ALF and IngaBritt och Arne Lundbergs Forskningsstiftelse grants to Michael Olausson and Stiftelsen Professor Lars-Erik Gelins Minnesfond grant to Debashish Banerjee.

Data availability

1. The raw/processed data required to reproduce few of the findings could not be shared at this time due to technical or time limitations. The experimental data required to reproduce the findings from this study will be made available to interested investigators upon request.
2. The Mass spectrometry proteomics data have been deposited to the ProteomeXchange Consortium *via* the PRIDE **[31]** with the dataset identifier PXD021179.
3. The code for all imaging pipelines for Cell and Area work will be made publicly available *via* github upon acceptance of the manuscript. During the review process we can also send the code to reviewers *via* e.g. a zip folder.

Declaration of interests

The authors declare that they have no known competing financial interests or personal relationships that could have appeared to influence the work reported in this paper.

Figure and Figure Legends

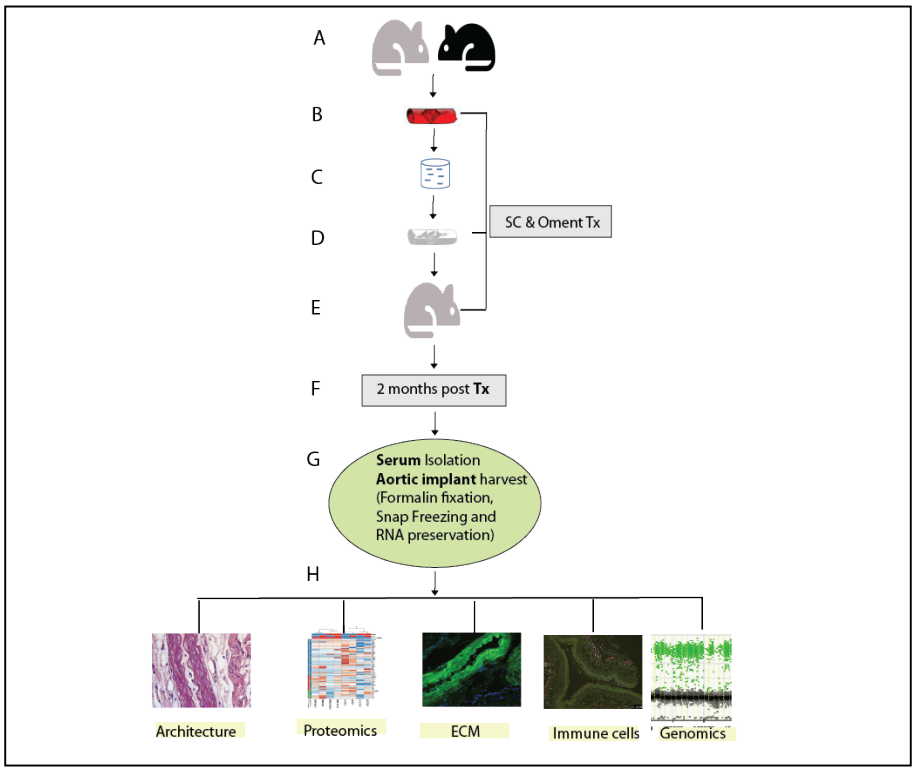

Figure 1. The experimental design and layout of the study. The experimental design is presented in a sequential layout **(A-H)**. Male Lewis and Brown Norway donor rats **(A)** were used for harvesting the aorta **(B)** as described in the Materials and Methods section. The aortas from donor rats (male Lewis/Brown Norway) were then perfused with chemical solution **(C)** to prepare a decellularized aortic scaffold **(D).** Implantations of the normal donor aorta **(B)** and decellularized aortas **(D)** at subcutaneous and omentum route were performed in female recipient mice **(E).** The implanted aortas and serum were collected following sacrifice of the recipient mice after 2 months, **(F)** for downstream processing for serum and tissues, **(G).** The tissue architecture, proteomics, ECM and genomic characterization were performed, **(H).**

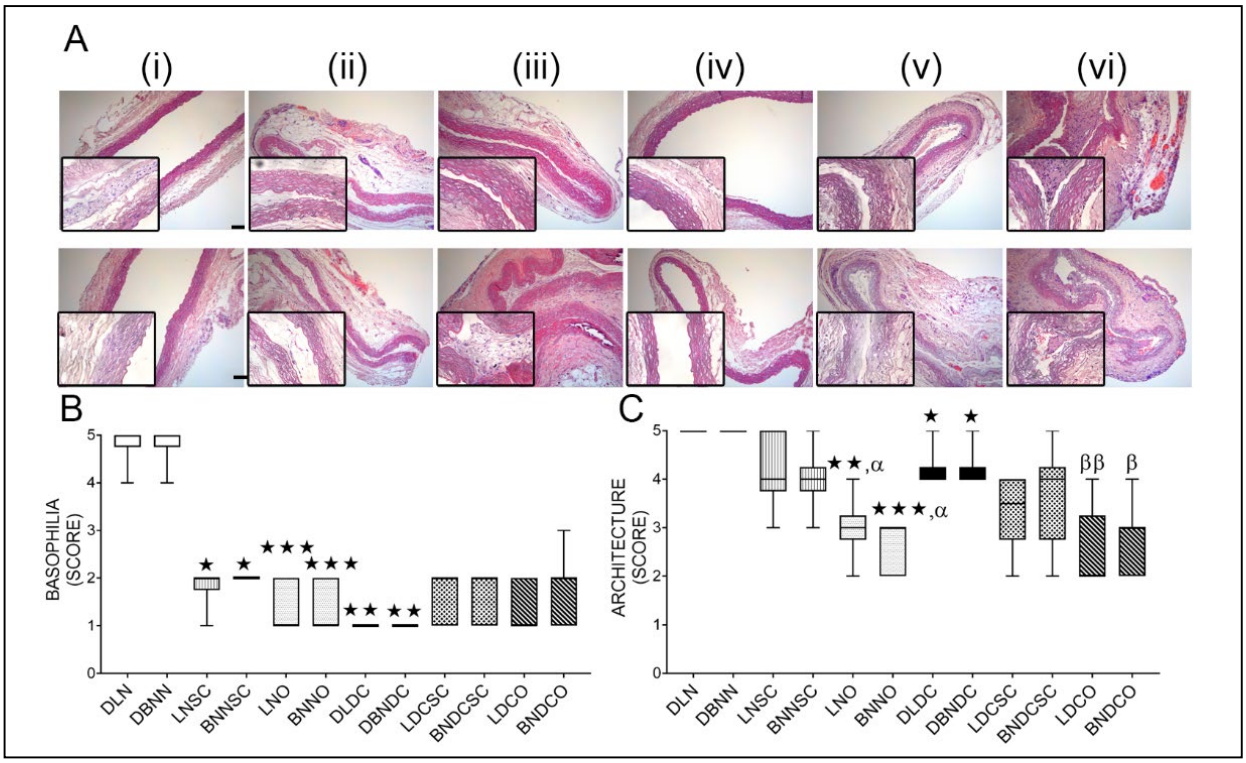

Figure 2. H&E staining of untreated and decellularized scaffolds before and after subcutaneous and omental implantation.

Figure 2A. Upper panel- Lewis and lower panel- Brown Norway donor normal and decellularized scaffolds and after implantation and harvest from subcutaneous and omentum route after 2 months. (i) normal (N), (ii) normal subcutaneous (NSC) (iii) normal omentum (NO), (iv) decellularized (DC), (v) decellularized subcutaneous (DCSC) and (vi) decellularized omentum (DCO).

All the donor scaffolds were stained with H&E and compared to the implanted aortas in terms of the Nuclear basophilia (B) and Architectural score (C). Representative images are shown at 10× magnification. Scale bars: 100 µm.

Figures 2B-C. The histological scoring system assesses the presence or removal of cells in terms of reduction of nuclear basophilic staining **(B)** and architecture preservation **(C)** of the scaffolds evaluated by a pathologist using a Comprehensive method of grading followed by Ordinal data measurements on a scale of 1 to 5 as defined in the Materials and Methods section. Results are presented as Maximum and minimum of the median (rank).

★$p<0.05$, ★★$p<0.01$ and ★★★$p<0.001$ indicates a significant difference in comparison to the respective untreated donor aorta; $^{\alpha}p<0.05$ and $^{\alpha\alpha}p<0.01$ indicates a significant difference in

comparison to the respective subcutaneous route by Kruskal-Wallis test followed by Dunn's Multiple Comparisons post hoc tests.

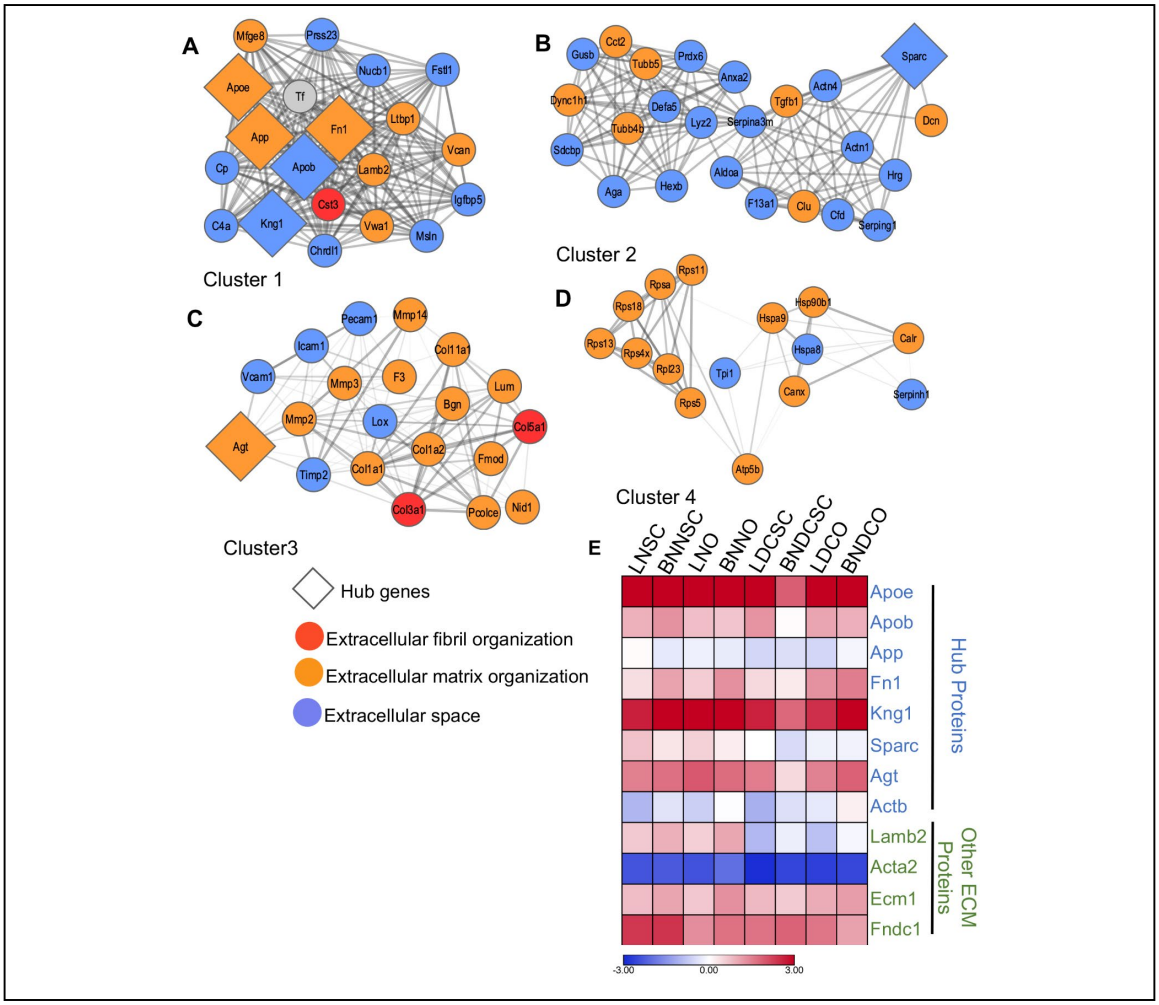

Figure 3. **The topological features of the ECM Network.**

The PPI network of the 8 hub and related proteins, created by quering the proteins enriched for ECM function against the STRING database. The network was exported and visualized using cytoscape. Proteins were then clustered with MCODE algorithm. Hub proteins were identified using Cytohubba app within the Cytoscape (A-D) MCODE cluster 1-4 respectively. Node color represents gene ontology terms and the edge width was proportional to the combined score based on STRING database. (E) Protein expression dynamics of the hub and selected ECM proteins showing heterogeneity within the transplanted groups. The colour scale represents the log2 normalized expression values.

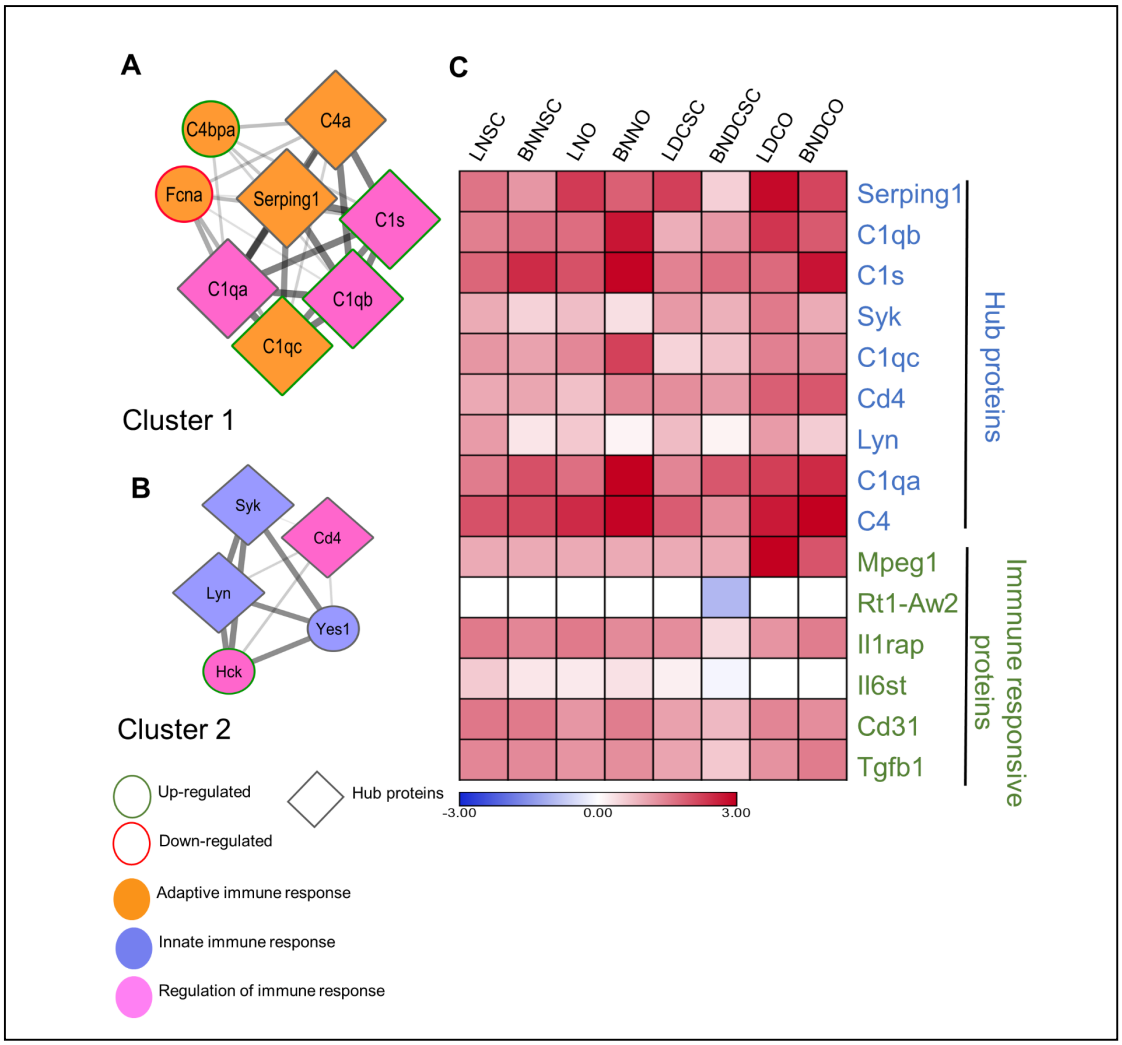

Figure 4. PPI network integration of the immune responsive proteins.

The PPI network was created by quering the proteins enriched for immune function against the STRING database. Network relationships derived from the STRING database were visualized with cytoscape. Proteins were then clustered with MCODE algorithm. Hub proteins were identified using cytohubba app within the cytoscape. **(A, B)** The top 2 MCODE clusters. Each node represents a protein and each edge denotes an interaction between a pair of proteins. Node color represents gene ontology terms and the thickness of the edge represents a larger combined-score derived from STRING database. **(C)** Protein expression dynamics of the hub and selected immune responsive proteins showing heterogeneity within the transplanted groups. The colour scale represents the log2 normalized expression values.

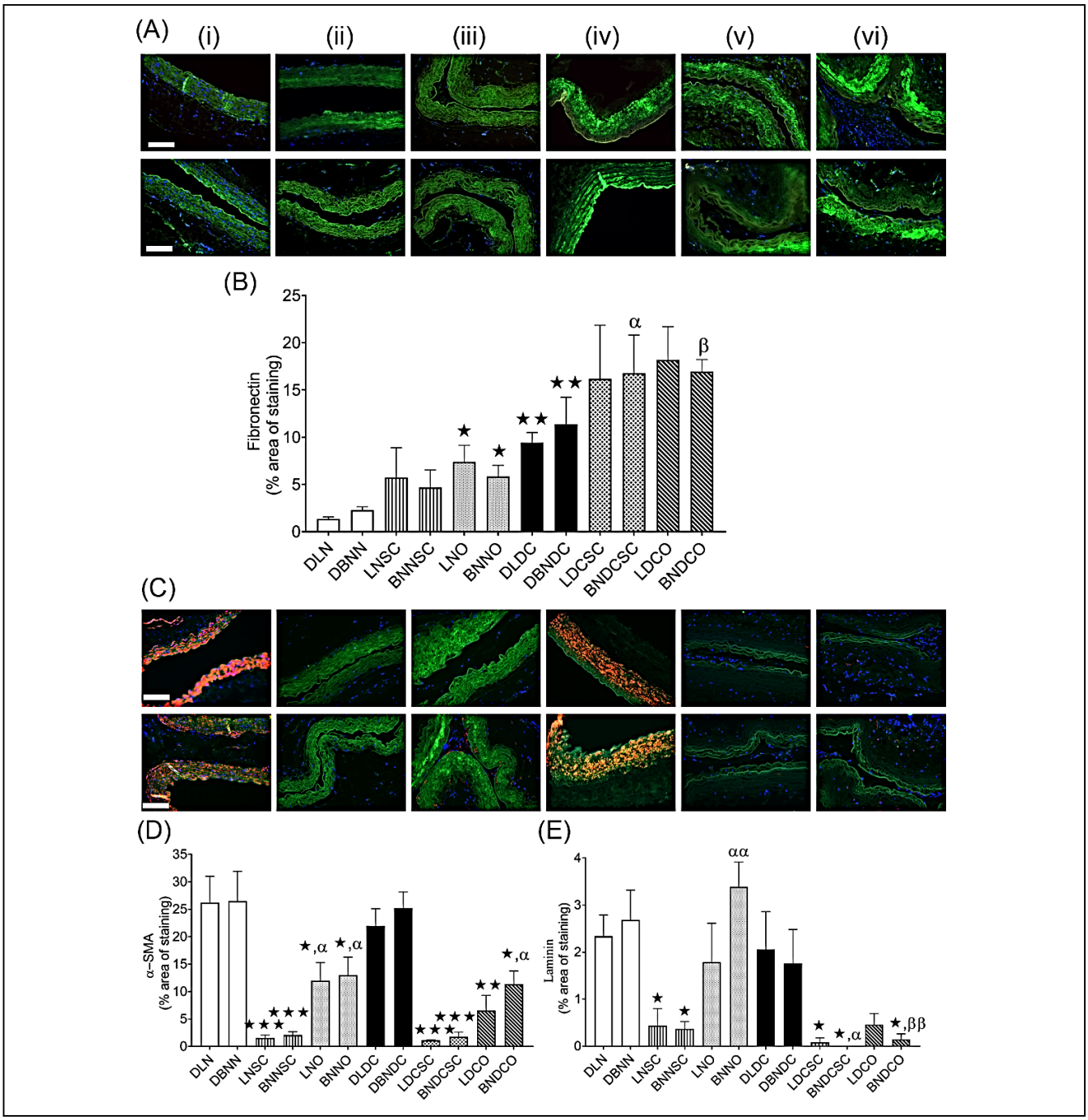

Figure 5. Immunohistostaining identifying expression of different ECM components following implantation of aortic scaffolds.

Implanted scaffolds after 2 months' time period were harvested from the subcutaneous and omentum site (implants) and analyzed by histological assessment of different ECM components. The upper panel denotes the implants from Lewis and lower panel from Brown Norway rats respectively.

A- Localization and B- Quantification of Fibronectin (green colour).

C- Localization and D-E- Quantification of α-SMA (red colour) and Laminin (green colour).

The overlapped images have been shown for clarity and localization of the cells.

Representative images are shown at 20x magnification. Scale bars: 100 µm.

Data are presented as Mean±SEM (n=6 in each group). ★p<0.05 and ★★p<0.01 indicates a significant difference in comparison to the respective untreated normal implant; αp<0.05 and βp<0.05 indicates a significant difference in comparison to the respective subcutaneous and omentum route by One way ANOVA followed by Tukey's post hoc test.

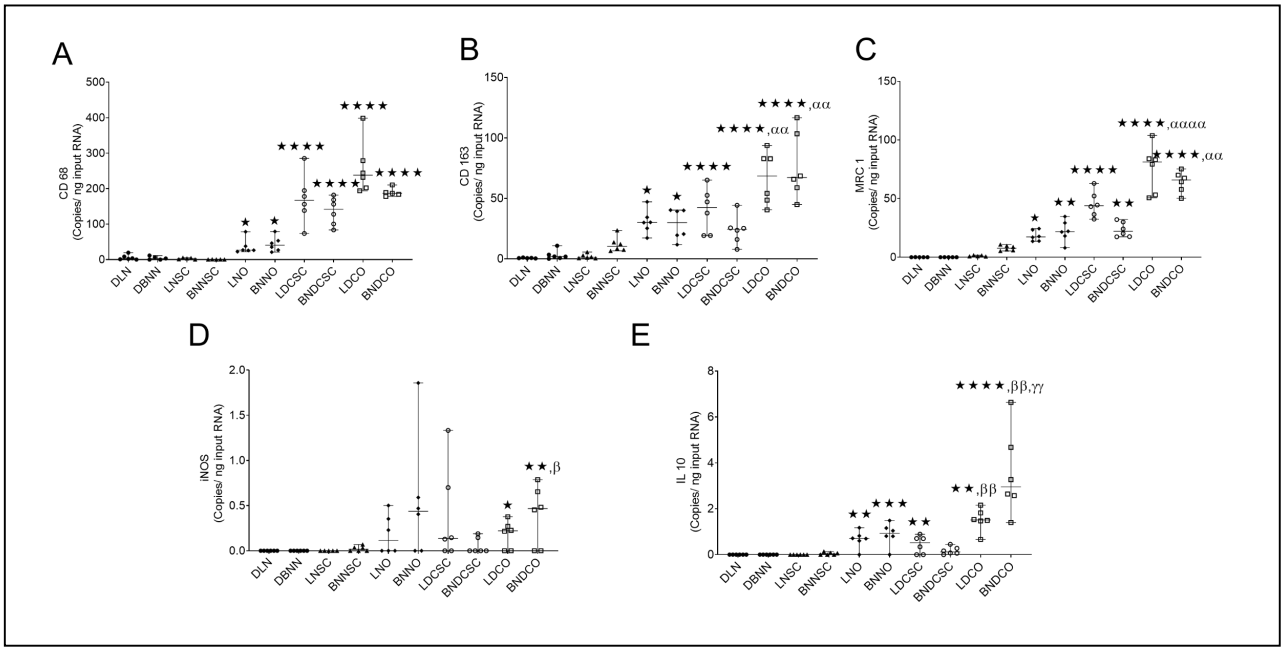

Figure 6. Gene expression analysis of different macrophage subsets following implantation.

Implanted scaffolds after 2 months' time period were harvested from the subcutaneous and omentum site and characterized by gene expression analysis for different macrophage (M1 *vs* M2 subsets).

A-E. Copies per ng input RNA of macrophage target gene were calculated using theoretical concentration of the target gene using reference gene, β-actin as outlined in the Materials and methods section. Data are shown as median and range of values (n=6 in each group).

★p<0.05, ★★p<0.01, ★★★p<0.001 and ★★★★p<0.0001 indicates a significant difference compared to the respective untreated normal implants; ααp<0.01 and ααααp<0.0001 indicates a significant difference in compared to the respective normal omentum implants, βp<0.05 and ββp<0.01 compared to the decellularized subcutaneous scaffold and γγp<0.01 compared to the decellularized syngeneic subcutaneous implants.

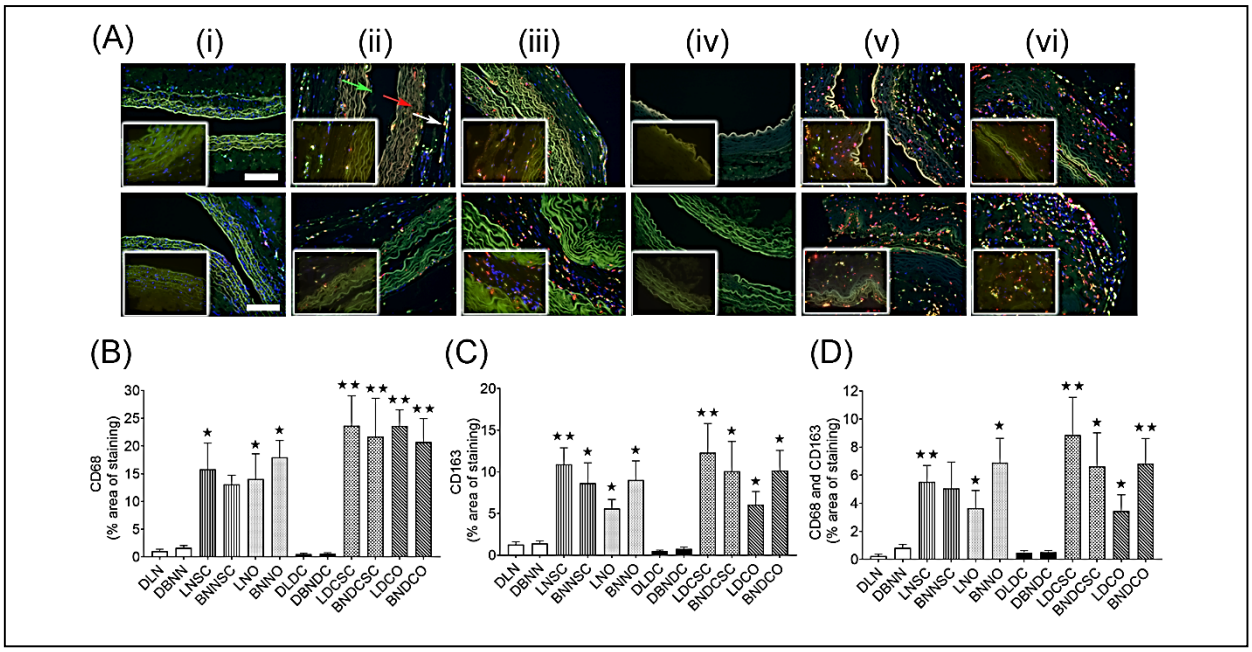

Figure 7. Immunohistostaining identifying macrophage subsets, CD68 and CD163 participating in the host response to implanted aortic scaffolds.

Implants after 2 months' time period were harvested from the subcutaneous and omentum site and analyzed by histological assessment for different macrophage subsets (M1 *vs* M2). The upper panel denotes the implants from Lewis and the lower panel from Brown Norway rats respectively. **Arrows**- red: CD68, green: CD163 and white- Both CD68 and CD163 colocalization.

7A- Localization and **7B-7D**- Quantification of CD68 and CD163 macrophages.

Data are presented as Mean±SEM (n=6 in each group). Representative images are shown at 20x magnification. Scale bars- 100 µm.

★$p<0.05$, ★★$p<0.01$ and ★★★$p<0.001$ indicates a significant difference in comparison to the respective donor normal scaffolds; $^{\alpha}p<0.05$ indicates a significant difference in comparison to the respective subcutaneous route by One way ANOVA followed by Tukey's post hoc test.

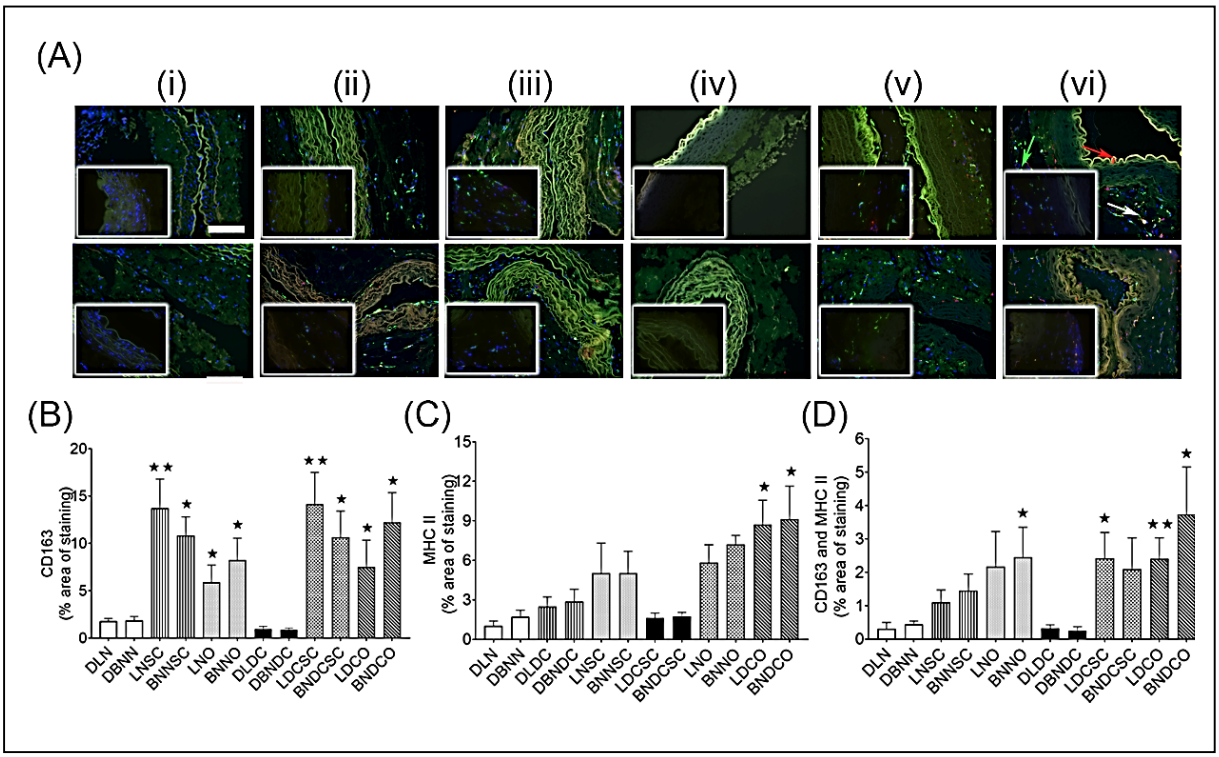

Figure 8. Immunohistostaining identifying macrophage subsets, CD163 and MHCII participating in the host response to implanted aortic scaffolds.

Implanted scaffolds after 2 months' time period were harvested from the subcutaneous and omentum site and compared with the normal and decellularized donor grafts by immunoohistological assessment for different macrophage subsets (M1 *vs* M2).

The upper panel denotes the implants from Lewis and the lower panel from Brown Norway rats respectively. **Arrows**- red: MHC II, green: CD163 and white- CD173 and MHC II colocalization.

8A- Localization and **8B-8D**- Quantification of CD163 and MHCII macrophages. Representative images are shown at 20x magnification. Scale bars: 100 µm.

Data are presented as Mean±SEM (n=6 in each group). ★$p<0.05$, ★★$p<0.01$ and ★★★$p<0.001$ indicates a significant difference in comparison to the respective untreated normal implant; $^{\alpha}p<0.05$ indicates a significant difference in comparison to the respective subcutaneous route by One way ANOVA followed by Tukey's post hoc test.

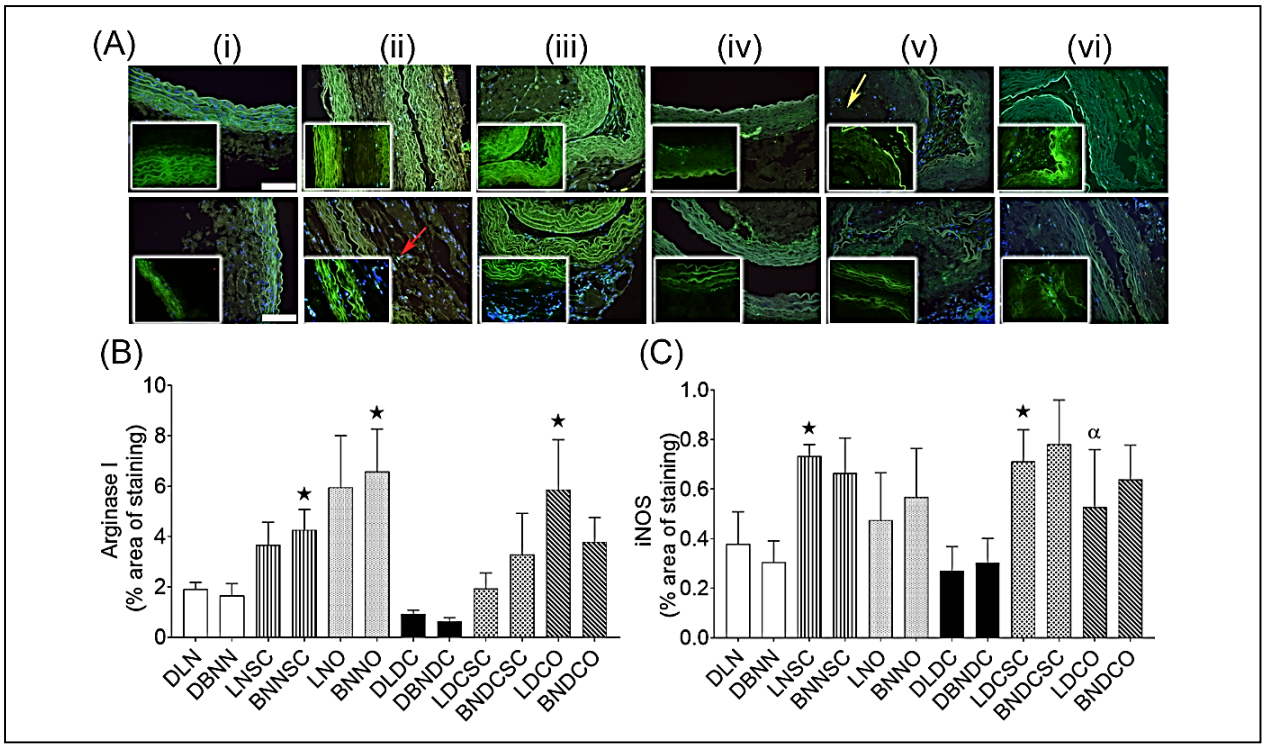

Figure 9. Immunohistostaining identifying macrophage subsets, Arginase I and iNOS participating in the host response to implanted aortic scaffolds.

Implanted scaffolds after 2 months' time period were harvested from the subcutaneous and omentum site and analyzed by histological assessment for different macrophage subsets (M1 *vs* M2). The upper panel denotes the implants from Lewis and the lower panel from Brown Norway rats respectively. 9A- Localization and 9B-9C- Quantification of Arginase I and iNOS macrophages. **Arrows**- red: iNOS and green: Arginase I.

Representative images are shown at 20x magnification. Scale bars: 100 µm. Data are presented as Mean±SEM (n=6 in each group). ★$p<0.05$, ★★$p<0.01$ and ★★★$p<0.001$ indicates a significant difference in comparison to the respective untreated normal implant; $^{\alpha}p<0.05$ indicates a significant difference in comparison to the respective subcutaneous route by One way ANOVA followed by Tukey's post hoc test.

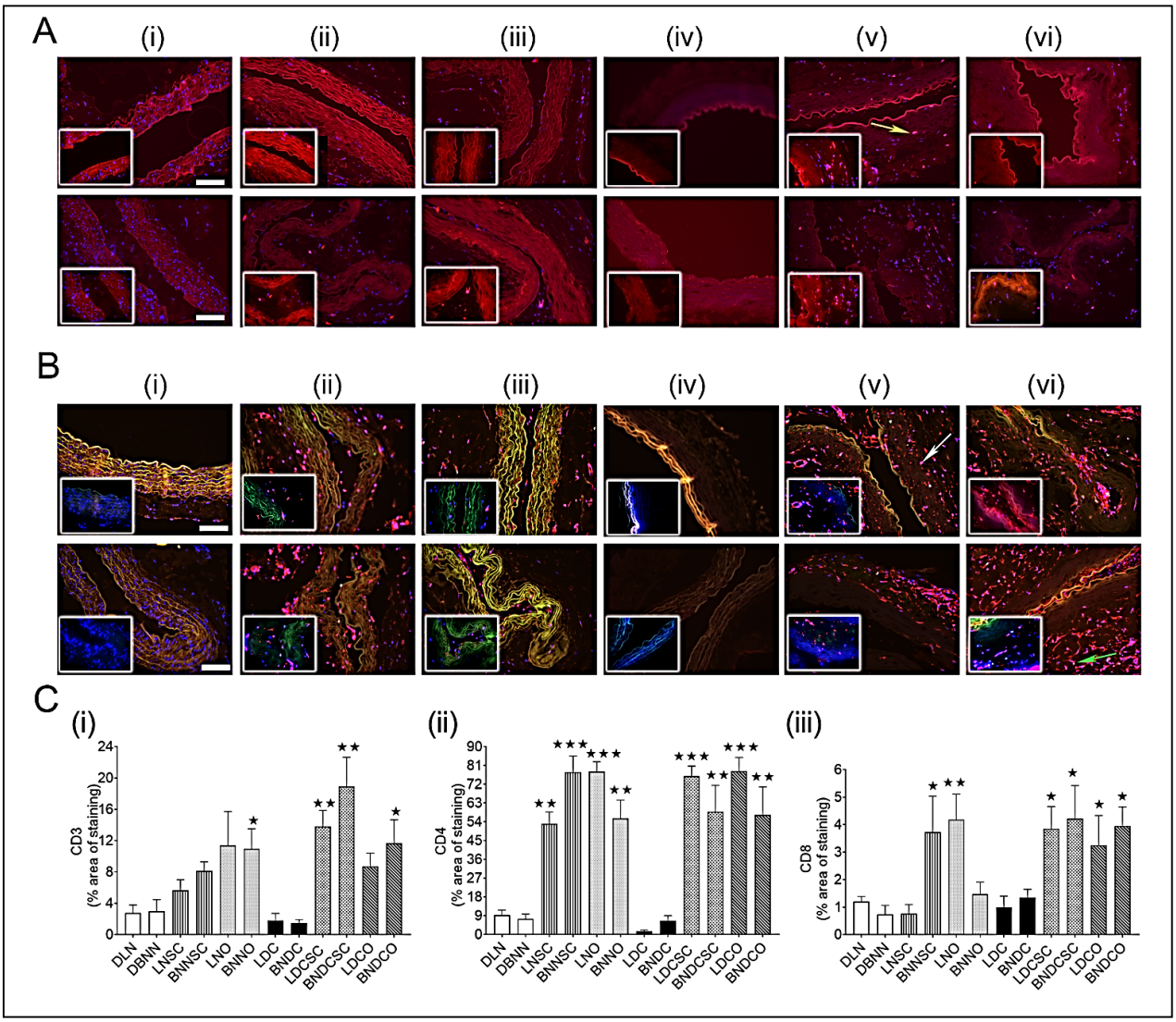

Figure 10. Immunostaining for immune markers, CD3, CD4 and CD8 in the implanted blood vascular scaffolds.

Implanted scaffolds after 2 months' time period were harvested from the subcutaneous and omentum site and analyzed by histological assessment for different immune markers (CD3+, CD4+ and CD8+ cells). The upper panel denotes the implants from Lewis and the lower panel from Brown Norway rats respectively. Yellow arrow denotes the presence of CD3+ve cells, white and green arrow denotes the presence of CD4+ve and CD8+ve cells respectively. Localization **(10A)** and quantification of CD3 (red colour) (**10C i**); Localization **(10B)** and quantification of CD4 (red colour) and CD8 (green colour) (**10C ii-iii)** is shown. Representative images are shown at 20x magnification. Scale bars: 100 µm. Data are presented as Mean±SEM (n=6 in each group). ★$p<0.05$, ★★$p<0.01$ and ★★★$p<0.001$ indicates a significant difference in comparison to the respective untreated normal implants by One-way ANOVA followed by Tukey's post hoc test.

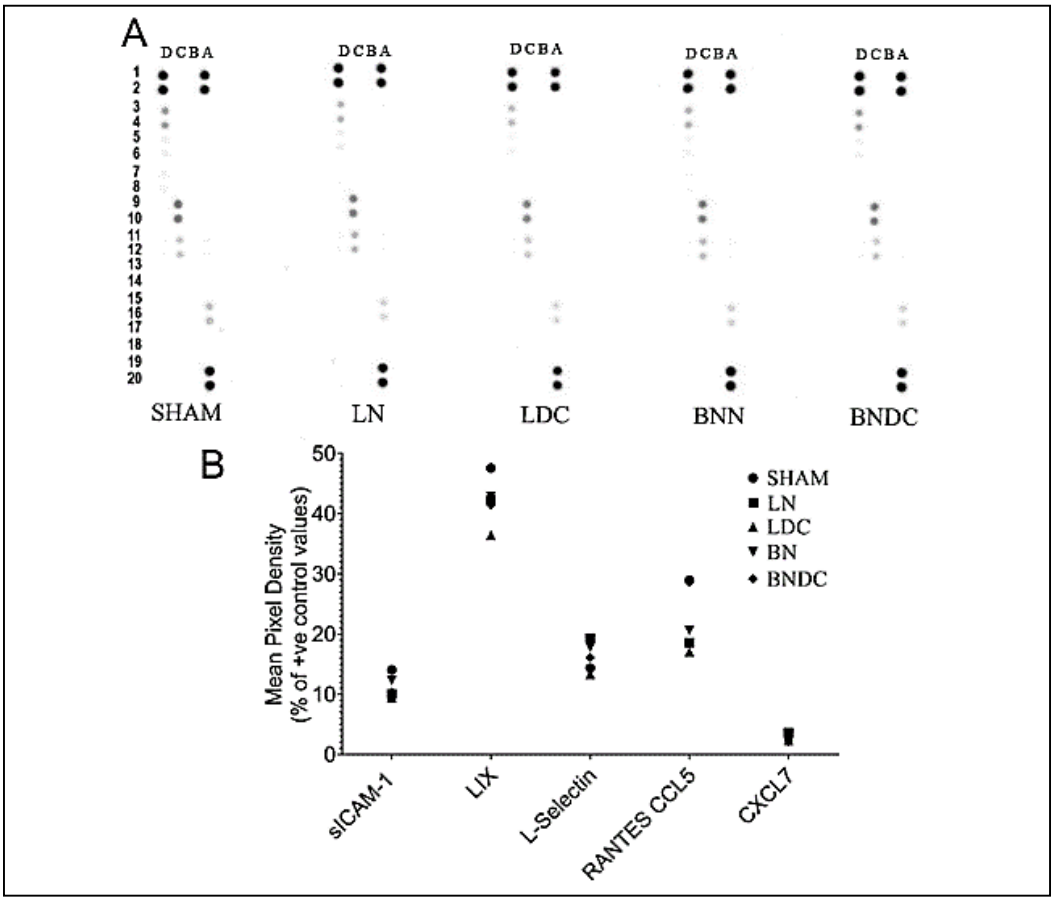

Figure 11. Cytokine and chemokine detection in serum of mice with and without implantation.

A. Membrane based proteome profiling of selected cytokines and chemokines. Serum from implanted recipient Lewis female mice (LN, LDC, BNN and BNDC) was compared with the Sham operated rats analyzed for the relative level of analytes as specified in the Materials and Methods section.

B. The calculated level of selected analytes showing most prominent expression for all the groups. The relative level of cytokines and chemokines was expressed as Mean Pixel Density after suitable correction of negative and positive reference spots present in the array membrane.

References

1. Weinberg, C. and E. Bell, *A blood vessel model constructed from collagen and cultured vascular cells.* Science, 1986. **231**(4736): p. 397-400.
2. Wu, P., et al., *Construction of vascular graft with circumferentially oriented microchannels for improving artery regeneration.* Biomaterials, 2020. **242**: p. 119922.
3. Burkel, W.E., et al., *Sequential studies of healing in endothelial seeded vascular prostheses: histologic and ultrastructure characteristics of graft incorporation.* J Surg Res, 1981. **30**(4): p. 305-24.
4. Olausson, M., et al., *Transplantation of an allogeneic vein bioengineered with autologous stem cells: a proof-of-concept study.* Lancet, 2012. **380**(9838): p. 230-7.
5. Caralt, M., et al., *Optimization and critical evaluation of decellularization strategies to develop renal extracellular matrix scaffolds as biological templates for organ engineering and transplantation.* Am J Transplant, 2015. **15**(1): p. 64-75.
6. Aamodt, J.M. and D.W. Grainger, *Extracellular matrix-based biomaterial scaffolds and the host response.* Biomaterials, 2016. **86**: p. 68-82.
7. Bloch, O., et al., *Immune response in patients receiving a bioprosthetic heart valve: lack of response with decellularized valves.* Tissue Eng Part A, 2011. **17**(19-20): p. 2399-405.
8. Mendoza-Novelo, B., et al., *Decellularization of pericardial tissue and its impact on tensile viscoelasticity and glycosaminoglycan content.* Acta Biomater, 2011. **7**(3): p. 1241-8.
9. Efendy, J.L., G.R. Campbell, and J.H. Campbell, *The effect of environmental cues on the differentiation of myofibroblasts in peritoneal granulation tissue.* J Pathol, 2000. **192**(2): p. 257-62.
10. Li, J., et al., *Improvement of tracheal autograft survival with transplantation into the greater omentum.* Ann Thorac Surg, 1995. **60**(6): p. 1592-6.
11. Tille, J.C., et al., *Histologic Assessment of Drug-Eluting Grafts Related to Implantation Site.* J Dev Biol, 2016. **4**(1).
12. Hsu, B.R.-S., S.-H. Fu, and A.Y.L. Wang, *Prolonged Survival of Subcutaneous Allogeneic Islet Graft by Donor Chimerism without Immunosuppressive Treatment.* International journal of endocrinology, 2017. **2017**: p. 7057852-7057852.
13. Platell, C., et al., *The omentum.* World J Gastroenterol, 2000. **6**(2): p. 169-176.
14. Smink, A.M., et al., *The Efficacy of a Prevascularized, Retrievable Poly(D,L,-lactide-co-epsilon-caprolactone) Subcutaneous Scaffold as Transplantation Site for Pancreatic Islets.* Transplantation, 2017. **101**(4): p. e112-e119.
15. Anderson, J.M., A. Rodriguez, and D.T. Chang, *Foreign body reaction to biomaterials.* Seminars in Immunology, 2008. **20**(2): p. 86-100.
16. Reid, B., et al., *PEG hydrogel degradation and the role of the surrounding tissue environment.* Journal of Tissue Engineering and Regenerative Medicine, 2015. **9**(3): p. 315-318.
17. Calle, E.A., et al., *Targeted proteomics effectively quantifies differences between native lung and detergent-decellularized lung extracellular matrices.* Acta Biomater, 2016. **46**: p. 91-100.
18. Pan, T.L., et al., *Expression, by functional proteomics, of spontaneous tolerance in rat orthotopic liver transplantation.* Immunology, 2004. **113**(1): p. 57-64.
19. Akhyari, P., et al., *The quest for an optimized protocol for whole-heart decellularization: a comparison of three popular and a novel decellularization technique and their diverse effects on crucial extracellular matrix qualities.* Tissue Eng Part C Methods, 2011. **17**(9): p. 915-26.
20. Crapo, P.M., T.W. Gilbert, and S.F. Badylak, *An overview of tissue and whole organ decellularization processes.* Biomaterials, 2011. **32**(12): p. 3233-43.
21. Gibson-Corley, K.N., A.K. Olivier, and D.K. Meyerholz, *Principles for valid histopathologic scoring in research.* Vet Pathol, 2013. **50**(6): p. 1007-15.
22. Wiśniewski, J.R., et al., *Universal sample preparation method for proteome analysis.* Nat Methods, 2009. **6**(5): p. 359-62.

23. Szklarczyk, D., et al., *STRING v10: protein-protein interaction networks, integrated over the tree of life.* Nucleic Acids Res, 2015. **43**(Database issue): p. D447-52.
24. Shannon, P., et al., *Cytoscape: a software environment for integrated models of biomolecular interaction networks.* Genome Res, 2003. **13**(11): p. 2498-504.
25. Assenov, Y., et al., *Computing topological parameters of biological networks.* Bioinformatics, 2008. **24**(2): p. 282-4.
26. Chin, C.H., et al., *cytoHubba: identifying hub objects and sub-networks from complex interactome.* BMC Syst Biol, 2014. **8 Suppl 4**(Suppl 4): p. S11.
27. Huang da, W., B.T. Sherman, and R.A. Lempicki, *Systematic and integrative analysis of large gene lists using DAVID bioinformatics resources.* Nat Protoc, 2009. **4**(1): p. 44-57.
28. Kanehisa, M., et al., *Data, information, knowledge and principle: back to metabolism in KEGG.* Nucleic Acids Res, 2014. **42**(Database issue): p. D199-205.
29. McDermott, G.P., et al., *Multiplexed target detection using DNA-binding dye chemistry in droplet digital PCR.* Anal Chem, 2013. **85**(23): p. 11619-27.
30. Coulter, S.J., *Mitigation of the effect of variability in digital PCR assays through use of duplexed reference assays for normalization.* Biotechniques, 2018. **65**(2): p. 86-91.
31. Perez-Riverol, Y., et al., *The PRIDE database and related tools and resources in 2019: improving support for quantification data.* Nucleic Acids Res, 2019. **47**(D1): p. D442-d450.
32. Tondreau, M.Y., et al., *Mechanical properties of endothelialized fibroblast-derived vascular scaffolds stimulated in a bioreactor.* Acta Biomater, 2015. **18**: p. 176-85.
33. Brasile, L., et al., *Pretransplant Kidney-Specific Treatment to Eliminate the Need for Systemic Immunosuppression.* Transplantation, 2010. **90**: p. 1294-8.
34. Methe, K.N., et al., *Differential Activation of Immune Cells for Genetically Different Decellularized Cardiac Tissues.* Tissue Eng Part A, 2020.
35. Schmitt, A., et al., *Optimized protocol for whole organ decellularization.* European Journal of Medical Research, 2017. **22**(1): p. 31.
36. Heath, D.E., *A Review of Decellularized Extracellular Matrix Biomaterials for Regenerative Engineering Applications.* Regenerative Engineering and Translational Medicine, 2019. **5**(2): p. 155-166.
37. Coito, A.J., et al., *The expression of extracellular matrix proteins during accelerated rejection of cardiac allografts in sensitized rats.* Transplantation, 1994. **57**(4): p. 599-605.
38. Black, F.M., et al., *The vascular smooth muscle alpha-actin gene is reactivated during cardiac hypertrophy provoked by load.* J Clin Invest, 1991. **88**(5): p. 1581-8.
39. Lambris, J.D., K.B. Reid, and J.E. Volanakis, *The evolution, structure, biology and pathophysiology of complement.* Immunol Today, 1999. **20**(5): p. 207-11.
40. Ricklin, D., et al., *Complement: a key system for immune surveillance and homeostasis.* Nat Immunol, 2010. **11**(9): p. 785-97.
41. Lin, C.M. and R.G. Gill, *Direct and indirect allograft recognition: pathways dictating graft rejection mechanisms.* Curr Opin Organ Transplant, 2016. **21**(1): p. 40-4.
42. Mills, C.D., et al., *M-1/M-2 macrophages and the Th1/Th2 paradigm.* J Immunol, 2000. **164**(12): p. 6166-73.
43. Juhas, M., et al., *Incorporation of macrophages into engineered skeletal muscle enables enhanced muscle regeneration.* Nature Biomedical Engineering, 2018. **2**(12): p. 942-954.
44. Graney, P.L., et al., *Macrophages of diverse phenotypes drive vascularization of engineered tissues.* Sci Adv, 2020. **6**(18): p. eaay6391.
45. Creemers, P., et al., *Evaluation of peripheral blood CD4 and CD8 lymphocyte subsets, CD69 expression and histologic rejection grade as diagnostic markers for the presence of cardiac allograft rejection.* Transpl Immunol, 2002. **10**(4): p. 285-92.
46. Gu, H., et al., *Bone regeneration in a rabbit ulna defect model: use of allogeneic adipose-derivedstem cells with low immunogenicity.* Cell Tissue Res, 2014. **358**(2): p. 453-64.

47. Piccotti, J.R., et al., *Are Th2 helper T lymphocytes beneficial, deleterious, or irrelevant in promoting allograft survival?* Transplantation, 1997. **63**(5): p. 619-24.
48. Zaiss, D.M., et al., *Amphiregulin enhances regulatory T cell-suppressive function via the epidermal growth factor receptor.* Immunity, 2013. **38**(2): p. 275-84.
49. Arpaia, N., et al., *A Distinct Function of Regulatory T Cells in Tissue Protection.* Cell, 2015. **162**(5): p. 1078-89.
50. Vlahos, A.E., N. Cober, and M.V. Sefton, *Modular tissue engineering for the vascularization of subcutaneously transplanted pancreatic islets.* Proc Natl Acad Sci U S A, 2017. **114**(35): p. 9337-9342.
51. Berman, D.M., et al., *Long-term survival of nonhuman primate islets implanted in an omental pouch on a biodegradable scaffold.* Am J Transplant, 2009. **9**(1): p. 91-104.
52. Brown, B.N., et al., *Macrophage phenotype and remodeling outcomes in response to biologic scaffolds with and without a cellular component.* Biomaterials, 2009. **30**(8): p. 1482-91.
53. Brown, B.N., et al., *Macrophage phenotype as a predictor of constructive remodeling following the implantation of biologically derived surgical mesh materials.* Acta Biomater, 2012. **8**(3): p. 978-87.
54. Gilbert, T.W., T.L. Sellaro, and S.F. Badylak, *Decellularization of tissues and organs.* Biomaterials, 2006. **27**(19): p. 3675-83.
55. Naso, F., et al., *Are FDA and CE sacrificing safety for a faster commercialization of xenogeneic tissue devices? Unavoidable need for legislation in decellularized tissue manufacturing.* Tissue Antigens, 2014. **83**(3): p. 193-4.